



ELSEVIER

Contents lists available at ScienceDirect

Journal of Theoretical Biology

journal homepage: www.elsevier.com/locate/yjtbi

The re-polarisation of M2 and M1 macrophages and its role on cancer outcomes

Nicoline Y. den Breems^{a,b,c}, Raluca Eftimie^{b,*}

^a Centre for Advanced Computational Solutions (C-fACS), Lincoln University, Lincoln 7476, New Zealand

^b Division of Mathematics, University of Dundee, Dundee DD1 4HN, United Kingdom

^c Division of Cancer Research, University of Dundee, Dundee DD1 9SY, United Kingdom

HIGHLIGHTS

- We introduce a mathematical model for interactions among tumour and M1&M2 macrophages.
- We investigate the dynamics of the model via simulations and sensitivity analysis.
- We show how the macrophage re-polarisation rates influence the ratio of M2/M1 cells.
- We discuss conditions under which the ratio M2/M1 can be used to predict tumour size.

ARTICLE INFO

Article history:

Received 22 February 2015

Received in revised form

8 October 2015

Accepted 19 October 2015

Keywords:

Cancer modelling

M1 and M2 macrophages

Th1 and Th2 immune cells

MSC: 92C50

ABSTRACT

The anti-tumour and pro-tumour roles of Th1/Th2 immune cells and M1/M2 macrophages have been documented by numerous experimental studies. However, it is still unknown how these immune cells interact with each other to control tumour dynamics. Here, we use a mathematical model for the interactions between mouse melanoma cells, Th2/Th1 cells and M2/M1 macrophages, to investigate the unknown role of the re-polarisation between M1 and M2 macrophages on tumour growth. The results show that tumour growth is associated with a type-II immune response described by large numbers of Th2 and M2 cells. Moreover, we show that (i) the ratio k of the transition rates k_{12} (for the re-polarisation $M1 \rightarrow M2$) and k_{21} (for the re-polarisation $M2 \rightarrow M1$) is important in reducing tumour population, and (ii) the particular values of these transition rates control the delay in tumour growth and the final tumour size. We also perform a sensitivity analysis to investigate the effect of various model parameters on changes in the tumour cell population, and confirm that the ratio k alone and the ratio of M2 and M1 macrophage populations at earlier times (e.g., day 7) cannot always predict the final tumour size.

© 2015 Published by Elsevier Ltd.

1. Introduction

The anti-tumour role of the immune system has been documented for more than a century (McCarthy, 2006). Despite recent success with some types of immunotherapies (e.g., involving antibodies or cancer vaccines), many anti-tumour therapies are still not leading to the expected outcomes (Rosenberg et al., 2004). One reason is that there are still numerous questions regarding the biological mechanisms behind the interactions between the immune cells and tumour cells. The complexity of these interactions is acknowledged by the immunoediting hypothesis, which emphasises the dual role of the immune response: tumour-

promoting and tumour-suppressing (Schreiber et al., 2011; Dunn et al., 2004). One of the mechanisms thought to be involved in the persistence and growth of tumours is the transition from a Th1- to a Th2-dominated environment, which appears to happen when the cancer microenvironment is dominated by cytokines such as IL-4 (synthesised by $CD4^+$ T cells) and growth factors like CSF1 and GM-CSF (Noy and Pollard, 2014). However, other studies have shown that both Th1- and Th2-dominated environments can successfully eliminate tumours independent of $CD8^+$ T cells (Nishimura et al., 1999; Hung et al., 1998; Perez-Diez et al., 2007), and in some cases the Th2-dominated environments are better at eliminating tumours compared to the Th1-dominated environments (Mattes et al., 2003). Overall, the mechanisms controlling the ratio of Th1/Th2 cells and its role on tumour elimination are still not completely understood.

A second ratio that seems to have predictive outcome on tumour growth and patient prognosis involves the M1 and M2

* Corresponding author.

E-mail addresses: nicoline.vanloenen@lincolnuni.ac.nz (N.Y. den Breems), r.a.eftimie@dundee.ac.uk (R. Eftimie).

<http://dx.doi.org/10.1016/j.jtbi.2015.10.034>

0022-5193/© 2015 Published by Elsevier Ltd.

macrophages (Ohri et al., 2009; Heusinkveld and van der Burg, 2011; Chen et al., 2011; Zhang et al., 2014). These macrophages were named after the Th1–Th2 cell nomenclature, despite the fact that there is actually a full spectrum of phenotypes between these two types of macrophage polarisation (Mantovani et al., 2004).

While many studies focused on the total numbers of tumour-infiltrating macrophages and their role on tumour growth and patient prognosis (Mattes et al., 2003; Zeni et al., 2007; Hammes et al., 2007; Bingle et al., 2002; Clear et al., 2010; Steidl et al., 2010), some of the results in these studies were contradictory (Heusinkveld and van der Burg, 2011). For example, several studies have shown that increased macrophage numbers correlate with poor patient prognosis (Bingle et al., 2002; Clear et al., 2010; Leek et al., 1996; Steidl et al., 2010; Zeni et al., 2007; Hammes et al., 2007; Zijlmans et al., 2006). Other studies have shown that increased macrophage numbers correlate with better patient survival (Welsh et al., 2005). Note that many of these contradictory results were for the same type of cancer: e.g., non-small cell lung cancer in Zeni et al. (2007) and Welsh et al. (2005). A possible explanation for these results is the type of macrophages that infiltrate the tumours: M1 versus M2 cells (Heusinkveld and van der Burg, 2011). However, detailed investigation of the phenotype of these tumour-infiltrating macrophages sometimes generated even more contradictory results. For example, Ohri et al. (2009) revealed that improved survival in patients with non-small cell lung cancer was associated with a higher density of M1 macrophages compared to M2 macrophages inside tumour islets (see Fig. 2(a) in Ohri et al., 2009). Moreover, the overall number of M1 and M2 macrophages was increased in patients with long survival times compared to patients with short survival times. In a different study, Ma et al. (2010) also showed an increase in the number of M1 macrophages inside islets of non-small lung cancers, for patients with improved survival. However, in contrast to the results in Ohri et al. (2009) and Ma et al. (2010) observed a slight decrease in the number of M2 macrophages in patients with long survival times compared to patients with short survival times (see Table 2 in Ma et al., 2010). Moreover, in Ma et al. (2010), improved survival was associated with similar M1 and M2 densities in tumour islets. One last difference between the studies in Ohri et al. (2009) and Ma et al. (2010), which was not emphasised by the authors themselves but can be deduced by comparing the data for macrophage densities inside tumour islets, is the ratio of M2/M1 in long-term survival patients (with $M2/M1 \approx 1$ in Ma et al., 2010 and $M2/M1 < 1$ in Ohri et al., 2009) and short-term survival patients (with $M2/M1 > 1$ in Ma et al., 2010 and $M2/M1 \approx 1$ in Ohri et al., 2009). Note that none of these studies did associate the number of macrophages with tumour size, but only with the percentage of patient survival.

To propose hypotheses regarding the biological mechanisms behind the observed discrepancies in experimental and clinical data, we need to have a better understanding of the interactions between the M1 and M2 macrophages and other cells in the microenvironment, such as the Th1 and Th2 cells with which the macrophages interact via type-I (e.g., IFN- γ , IL-12) and type-II (e.g., IL-4, IL-10) cytokines (Biswas and Mantovani, 2010).

While there are mathematical models that focus on the Th2/Th1 balance (Kogan et al., 2013; Kim et al., 2013; Gross et al., 2011; Eftimie et al., 2010) and models that focus on the M2/M1 balance (Wang et al., 2012; Louzoun et al., 2014) in various immunological contexts, including cancer immunotherapies, there are no mathematical models that combine these two aspects.

The goal of this study is to investigate whether the variation in the M2/M1 ratio and the re-polarisation of macrophages accounts for the difference in tumour growth or tumour decay. To this end, we derive a new non-spatial mathematical model that describes the interactions between the tumour cells (which can be

recognised or not by the immune cells) and two types of immune cells, namely macrophages (M1 and M2) and T helper (Th1 and Th2) cells. For the macrophages dynamics, we explicitly model the plasticity of these cells that can re-polarise into a M1 or M2 phenotype depending on the cytokine environment (i.e., type I cytokines such as IFN- γ can lead to M1 macrophages, while type-II cytokines such as IL-10 can lead to M2 macrophages). While this model cannot address any questions regarding the spatial aspects of tumour-immune interactions, it offers a much simpler framework within which we can investigate these interactions. We then use this mathematical model to investigate the effect of the ratio M2/M1 on tumour growth for early and advanced tumours. We first investigate all possible steady states, and study the role of the ratio $k = k_{12}/k_{21}$ of the re-polarisation rates between the M1 and M2 macrophages on these states and their stability. Next we investigate numerically the role of model parameters on the long-term dynamics of the tumour growth. Since the numerical results depend on various parameters, we also conduct a sensitivity analysis to decide which parameters are most likely to influence the tumour growth. Our analysis reveals that a ratio $M2/M1 > 1$ can explain the growth in tumour size. However, for $M2/M1 < 1$, the variation in tumour growth cannot be explained by this ratio alone (see the discussion in Section 5.4).

We emphasise from the beginning that the results of this study depend on the mice experimental data we used to parametrise the model. In particular, we use mice melanoma data from Chen et al. (2011) since it shows multiple time points and thus allows for better model parametrisation (as opposed to the data in Ohri et al., 2009; Ma et al., 2010 for small-cell lung cancers, that shows only one time point). While it will be interesting to investigate how the results change if we use human data, such an investigation is beyond the scope of current study.

The article is structured as follows. In Section 2 we describe in detail the new mathematical model for tumour-immune interactions. In Section 3 we investigate the steady states of this model, and their stability. In Section 4 we study the dynamics of the model using numerical simulations. In Section 5 we perform a sensitivity analysis for the parameters and initial conditions of the model. We conclude in Section 6 with a summary and discussion of the results.

2. Model description

Throughout this paper, we model and investigate the interactions of tumour cells (x_T) with macrophages (x_M) and Th cells (x_{Th}). For the immune response, we model separately the dynamics of Th1 (x_{Th1}) and Th2 (x_{Th2}) cells, as well as the dynamics of M1 (x_{M1}) and M2 (x_{M2}) macrophages. For the tumour cells, we model the dynamics of immunogenic tumour cells (x_{Ts}) that can be recognised (i.e., “seen”) by the immune cells and non-immunogenic tumour cells (x_{Tn}) that escape the surveillance by the immune system. To keep our mathematical model relatively simple, we will not model explicitly the type-I and type-II cytokines that mediate the interactions between M1 and Th1 cells, and between M2 and Th2 cells. These cytokine-mediated interactions will be modelled implicitly, by assuming that the cytokines are produced by the macrophages and the Th cells. Thus, the time-evolution of all these cell densities is given by:

$$\frac{dx_{Tn}}{dt} = rx_{Tn} \left(1 - \frac{x_{Tn} + x_{Ts}}{\beta_T} \right) + k_{sn}x_{Ts} - \delta_{mn}x_{M1}x_{Tn} + r_{mn}x_{Tn}x_{M2}, \quad (1a)$$

$$\frac{dx_{Ts}}{dt} = rx_{Ts} \left(1 - \frac{x_{Tn} + x_{Ts}}{\beta_T} \right) - k_{sn}x_{Ts} - \delta_{ms}x_{M1}x_{Ts} - \delta_{ts}x_{Ts}x_{Th1}, \quad (1b)$$

$$\frac{dx_{M1}}{dt} = (a_s x_{Ts} + a_{m1} x_{Th1}) x_{M1} \left(1 - \frac{x_{M1} + x_{M2}}{\beta_M}\right) - \delta_{m1} x_{M1} - k_{12} x_{M1} x_{M2} + k_{21} x_{M1} x_{M2}, \quad (1c)$$

$$\frac{dx_{M2}}{dt} = (a_n x_{Tn} + a_{m2} x_{Th2}) x_{M2} \left(1 - \frac{x_{M1} + x_{M2}}{\beta_M}\right) - \delta_{m2} x_{M2} + k_{12} x_{M1} x_{M2} - k_{21} x_{M1} x_{M2}, \quad (1d)$$

$$\frac{dx_{Th1}}{dt} = a_{h1} x_{M1} + r_{h1} x_{M1} x_{Th1} \left(1 - \frac{x_{Th1} + x_{Th2}}{\beta_{Th}}\right) - \delta_{h1} x_{Th1}, \quad (1e)$$

$$\frac{dx_{Th2}}{dt} = a_{h2} x_{M2} + r_{h2} x_{M2} x_{Th2} \left(1 - \frac{x_{Th1} + x_{Th2}}{\beta_{Th}}\right) - \delta_{h2} x_{Th2}. \quad (1f)$$

These equations incorporate the following biological assumptions:

- Both tumour cell populations proliferate logistically at a rate r , to account for the slow-down in tumour growth due to lack of nutrients, as observed experimentally (Diefenbach et al., 2001; Laird, 1964). The x_{Ts} cells can mutate at a rate k_{sn} and become x_{Tn} cells. Also, the x_{Ts} cells can be eliminated at a rate δ_{ts} by the adaptive immune response represented by the Th1 cells (Hung et al., 1998). Moreover, experimental studies have shown that the nonspecific macrophage reaction following the inoculation of tumour cells leads to the production of nitric oxide (cytotoxic for tumours; Xu et al., 2002) in both immunogenic and non-immunogenic tumours (Kisseleva et al., 2001). Thus, we make the assumption that the M1 macrophages could eliminate the x_{Tn} cells at a rate δ_{mn} and x_{Ts} cells at a rate δ_{ms} , where we choose $\delta_{mn} = \delta_{ms}$; see Table A2. Moreover, we assume that the x_{Tn} cells can proliferate in the presence of M2 cells (Mills, 2012) at a rate r_{mn} . Even if the extracellular signals released by M2 cells could contribute also to the growth of x_{Ts} cells, the large mutation rate of mouse melanoma (Cillo et al., 1987) will lead to a fast transition from x_{Ts} to x_{Tn} cells. Thus, for this study, we decided to ignore the potential contribution of x_{M2} macrophages to the growth of x_{Ts} cancer cells. Finally, we assume that the tumour cells die at rate much lower compared to the immune cells, and thus we ignore the natural death rate of x_{Tn} and x_{Ts} cells.
- The M1 macrophages proliferate at rate a_s in the presence of x_{Ts} tumour-specific antigens, and at rate a_{m1} in the presence of type I cytokines (which can be produced by Th1 cells, once these cells become activated) (Mantovani et al., 2004). Moreover the M1 macrophages have a half-life of $1/\delta_{m1}$. In addition, the cross-talk between the M1 and M2 macrophage-polarising signalling pathways can lead to a re-polarisation, at rate k_{12} , of M1 cells into M2 cells (Sica and Bronte, 2007).
- The M2 macrophages proliferate at rate a_n in the presence of cytokines and growth factors produced by x_{Tn} cells, and at rate a_{m2} in the presence of type II cytokines (e.g., IL-4, which can be produced by Th2 cells, once these cells become activated) (Mantovani et al., 2004; Gordon and Martinez, 2010). The half-life of M2 macrophages is $1/\delta_{m2}$. For simplicity, throughout this study we will assume that $\delta_{m2} = \delta_{m1}$. Finally, the cross-talk between the M1 and M2 cells can lead to a re-polarisation, at rate k_{21} , of M2 macrophages into M1 macrophages (Sica and Bronte, 2007).
- The Th1 cells are activated, at rate a_{h1} , by type-I cytokines (e.g., IFN- γ) that can be produced by the M1 macrophages (Romagnani, 1999; Sica and Mantovani, 2012). Also, they proliferate at rate r_{h1} in the presence of type-I cytokines produced by M1 cells, and have a half-life of $1/\delta_{h1}$.
- The Th2 cells are activated, at rate a_{h2} , by type-II cytokines that can be produced by the M2 macrophages (Romagnani, 1999; Sica and Mantovani, 2012). These Th cells proliferate at rate r_{h2}

in the presence of type-II cytokines produced by the M2 cells, and have a half-life of $1/\delta_{h2}$.

Note that the terms that appear in model (1) are one of the multiple possible ways of describing the dynamics of tumour and immune cells. There are various models in the mathematical literature, where the growth and interaction rates of cells are assumed linear (not depending on direct or indirect interactions with other cells); see, for example, Louzoun et al. (2014). Nevertheless, the goal of our study is not to investigate all these possible modelling approaches; rather is to choose one way of describing the interactions, and use it to investigate the anti-tumour type-I and type-II immune responses.

3. Steady states and their stability

To investigate the dynamics of system (1), we first focus on its long-term behaviour as described by the number and stability of the steady states. By calculating these states, we aim to emphasise the complex dynamics of Eqs. (1), and the difficulty of fully understanding this dynamics.

3.1. Tumour-free steady states

We first study the case when $x_{Tn} = x_{Ts} = 0$. For the baseline parameter values used here and listed in Table A2, these tumour-free states are generally unstable (see the discussion in Appendix C). We therefore expect the dynamics of system (1) to move away from these states – as it will be confirmed in Sections 4 and 5 by the numerical simulations:

- Tumour-Free Immune-Free (TFIF) state:**

$$(x_{Tn}^*, x_{Ts}^*, x_{M1}^*, x_{M2}^*, x_{Th1}^*, x_{Th2}^*) = (0, 0, 0, 0, 0, 0).$$

- Tumour-Free Type-I Immune response Present (TF1IP) state:**

$$(x_{Tn}^*, x_{Ts}^*, x_{M1}^*, x_{M2}^*, x_{Th1}^*, x_{Th2}^*) = (0, 0, x_{M1}^*, 0, x_{Th1}^*, 0),$$

with x_{M1}^* and x_{Th1}^* given implicitly by the following equations:

$$x_{M1}^* = \frac{\delta_{h1} x_{Th1}^*}{a_{h1} + r_{h1} x_{Th1}^* \left(1 - \frac{x_{Th1}^*}{\beta_{Th}}\right)} \quad \text{and} \quad x_{Th1}^* = \frac{\delta_{m1}}{a_{m1} \left(1 - \frac{x_{M1}^*}{\beta_M}\right)}. \quad (2)$$

For the parameter values used throughout this paper and given in Table A2, there is a unique TF1IP steady state (see Appendix B).

- Tumour-Free Type-II Immune response Present (TF2IP) state:**

$$(x_{Tn}^*, x_{Ts}^*, x_{M1}^*, x_{M2}^*, x_{Th1}^*, x_{Th2}^*) = (0, 0, 0, x_{M2}^*, 0, x_{Th2}^*),$$

with

$$x_{M2}^* = \frac{\delta_{h2} x_{Th2}^*}{a_{h2} + r_{h2} x_{Th2}^* \left(1 - \frac{x_{Th2}^*}{\beta_{Th}}\right)} \quad \text{and} \quad x_{Th2}^* = \frac{\delta_{m2}}{a_{m2} \left(1 - \frac{x_{M2}^*}{\beta_M}\right)}. \quad (3)$$

This state is also unique (see Appendix B).

- Tumour-Free Type-I and Type-II Immune-Present (TFIP) states:**

$$(x_{Tn}, x_{Ts}, x_{M1}, x_{M2}, x_{Th1}, x_{Th2}) = (0, 0, x_{M1}^*, x_{M2}^*, x_{Th1}^*, x_{Th2}^*),$$

with x_{M1}^* , x_{M2}^* , x_{Th1}^* , x_{Th2}^* given implicitly by the following relations:

$$x_{M1}^* = \frac{\delta_{h1} x_{Th1}^*}{a_{h1} + r_{h1} x_{Th1}^* \left(1 - \frac{x_{Th1}^* + x_{Th2}^*}{\beta_{Th}}\right)},$$

$$x_{M2}^* = \frac{\delta_{h2} x_{Th2}^*}{a_{h2} + r_{h2} x_{Th2}^* \left(1 - \frac{x_{Th1}^* + x_{Th2}^*}{\beta_{Th}}\right)}, \quad (4a)$$

$$x_{Th1}^* = \frac{\delta_{m1} + k_{12} x_{M2}^* - k_{21} x_{M1}^*}{a_{m1} \left(1 - \frac{x_{M1}^* + x_{M2}^*}{\beta_M}\right)}, \quad x_{Th2}^* = \frac{\delta_{m2} - k_{12} x_{M1}^* + k_{21} x_{M1}^*}{a_{m2} \left(1 - \frac{x_{M1}^* + x_{M2}^*}{\beta_M}\right)}. \quad (4b)$$

In contrast to the TF1IP and TF2IP states that are unique, there is an infinite number of TFIP states – see Fig. B1(A) in Appendix B. This emphasises the complexity of system (1), and the difficulty to predict its dynamics.

3.2. Tumour-present steady states

Next, we discuss the states where $x_{Tn} > 0$. Note that if $x_{Tn} = 0$, then we have also $x_{Ts} = 0$. The stability of the steady states with $x_{Ts} = 0$ is discussed in Appendix C. The case $x_{Ts} \neq 0$ is more complicated and it is very difficult to investigate analytically:

- **Tumour-only (TO) states:**

$$(x_{Tn}^*, x_{Ts}^*, x_{M1}^*, x_{M2}^*, x_{Th1}^*, x_{Th2}^*) = (x_{Tn}^*, \beta_T - x_{Tn}^*, 0, 0, 0, 0),$$

where for $x_{Ts}^* = 0$ we have $x_{Tn}^* = \beta_T$. For the baseline parameter values used in this paper and described in Table A2, these states are always unstable (see Appendix C). Thus the dynamics of system (1) will never approach the TO states.

- **Tumour-Present Type-1 Immune Response Present (TP1IP) states:**

$$(x_{Tn}^*, x_{Ts}^*, x_{M1}^*, x_{M2}^*, x_{Th1}^*, x_{Th2}^*) = (x_{Tn}^*, 0, x_{M1}^*, 0, x_{Th1}^*, 0),$$

with

$$x_{Tn}^* = \frac{\beta_T (r - \delta_{mn} x_{M1}^*)}{r}, \quad (5a)$$

$$x_{M1}^* = \frac{\delta_{h1} x_{Th1}^*}{a_{h1} + r_{h1} x_{Th1}^* \left(1 - \frac{x_{Th1}^*}{\beta_{Th}}\right)}, \quad x_{Th1}^* = \frac{\delta_{m1}}{a_{m1} \left(1 - \frac{x_{M1}^*}{\beta_M}\right)}. \quad (5b)$$

For the baseline parameter values used in this paper, the TP1IP state is unique (see Appendix B). Moreover this state is unstable and the dynamics of system (1) will not evolve towards it (see Appendix C).

- **Tumour-Present Type-II Immune Response Present (TP2IP) states:**

$$(x_{Tn}^*, x_{Ts}^*, x_{M1}^*, x_{M2}^*, x_{Th1}^*, x_{Th2}^*) = (x_{Tn}^*, 0, 0, x_{M2}^*, 0, x_{Th2}^*),$$

with

$$x_{Tn}^* = \frac{\beta_T (r + r_{mn} x_{M2}^*)}{r}, \quad (6a)$$

$$x_{M2}^* = \frac{\delta_{h2} x_{Th2}^*}{a_{h2} + r_{h2} x_{Th2}^* \left(1 - \frac{x_{Th2}^*}{\beta_{Th}}\right)}, \quad x_{Th2}^* = \frac{\delta_{m2} - a_n x_{Tn}^* \left(1 - \frac{x_{M2}^*}{\beta_M}\right)}{a_{m2} \left(1 - \frac{x_{M2}^*}{\beta_M}\right)}. \quad (6b)$$

Also this state is unique and stable for the parameter values used in this paper – as confirmed by the numerical simulations in Fig. 3.

- **Tumour-Present Immune-Present (TPIP) states:**

$$(x_{Tn}^*, x_{Ts}^*, x_{M1}^*, x_{M2}^*, x_{Th1}^*, x_{Th2}^*),$$

with $x_{Ts}^* = 0$ or $x_{Ts}^* > 0$. As we will see throughout the next sections, for the parameter values used in this paper, system (1) usually approaches a TPIP state with $x_{Ts}^* = 0$. We emphasise here that the TPIP states are not unique, as shown in Fig. B1(B). The existence of these multiple states makes it difficult to

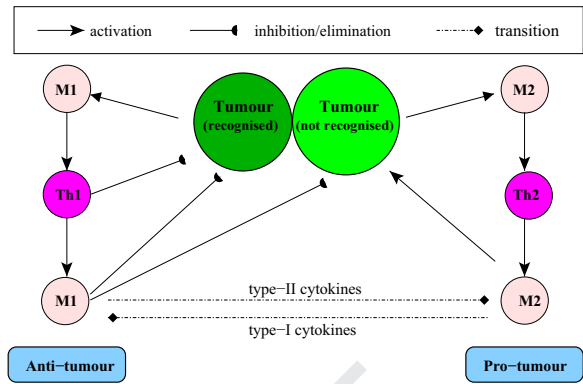


Fig. 1. Schematic description of possible tumour-immune interactions, as suggested by various experimental results (Mattes et al., 2003; Mantovani et al., 2008; Baba et al., 2008; Biswas and Mantovani, 2010).

investigate analytically their stability. However, the numerical results in the next sections suggest that the stability of these states depends also on the ratio $k = k_{12}/k_{21}$.

4. Numerical results

Next, we study the dynamics of model (Fig. 1) through numerical simulations using ODE23tb in MATLAB 2013b. Since we want to understand the mechanisms behind the change in the M2/M1 ratio, we fit several model parameters to experimental data from Chen et al. (2011), who focused on melanoma studies in mice (see Fig. 2). In particular we study numerically the effect of injecting on day zero 10^6 x_{Ts} tumour cells and 10^3 x_{Tn} tumour cells. We also assume that $x_{Th1}(0) = 0$, $x_{Th2}(0) = 0$ (i.e., no activated immune cells at the time of the injection). However, a small number of tissue macrophages can be present at the injection site: $x_{M1}(0) = 100$ and $x_{M2}(0) = 100$. For an extended overview of the model variables and parameters, and a description of the experimental setup see Appendix A.1 and Tables A1 and A2. Fig. 2 (A) compares the dynamics of $x_{Tn} + x_{Ts}$ cells with tumour data from Chen et al. (2011), to identify the parameter values for tumour growth. Fig. 2(B) compares the numbers of x_{M1} and x_{M2} cells on days 7 and 14 with macrophages data from Chen et al. (2011) (to identify parameter values that govern the macrophage dynamics; see also Appendix A).

Fig. 3 shows the dynamics of tumour and immune cells, for the parameter values identified through comparison with the data (see Tables A1 and A2). We first notice that the x_{Tn} cells grow to the carrying capacity while the x_{Ts} cells are eliminated (Fig. 3(A)). Moreover, as seen in the experimental results (Fig. 2(B)), there is a shift in the macrophage profile: from a x_{M1} profile for $t < 10$ days to a x_{M2} profile for $t > 10$ days (Fig. 3(B)). This shift is accompanied by a shift in the Th profile: from a Th1-dominated dynamics during the first ≈ 15 days (Fig. 3(C)) to a Th2-dominated dynamics at a later time (Fig. 3(D)). Finally, we emphasise that for these particular parameter values, the long-term dynamics of model (1) approaches the TP2IP steady state; see Eqs. (6).

5. Sensitivity analysis

Even if we estimated some parameter values using tumour and macrophages data from Chen et al. (2011), other parameters values were guessed. To ensure that the general conclusions of the model are still valid if we change slightly the model parameters and the initial conditions of the simulations, we perform a local sensitivity

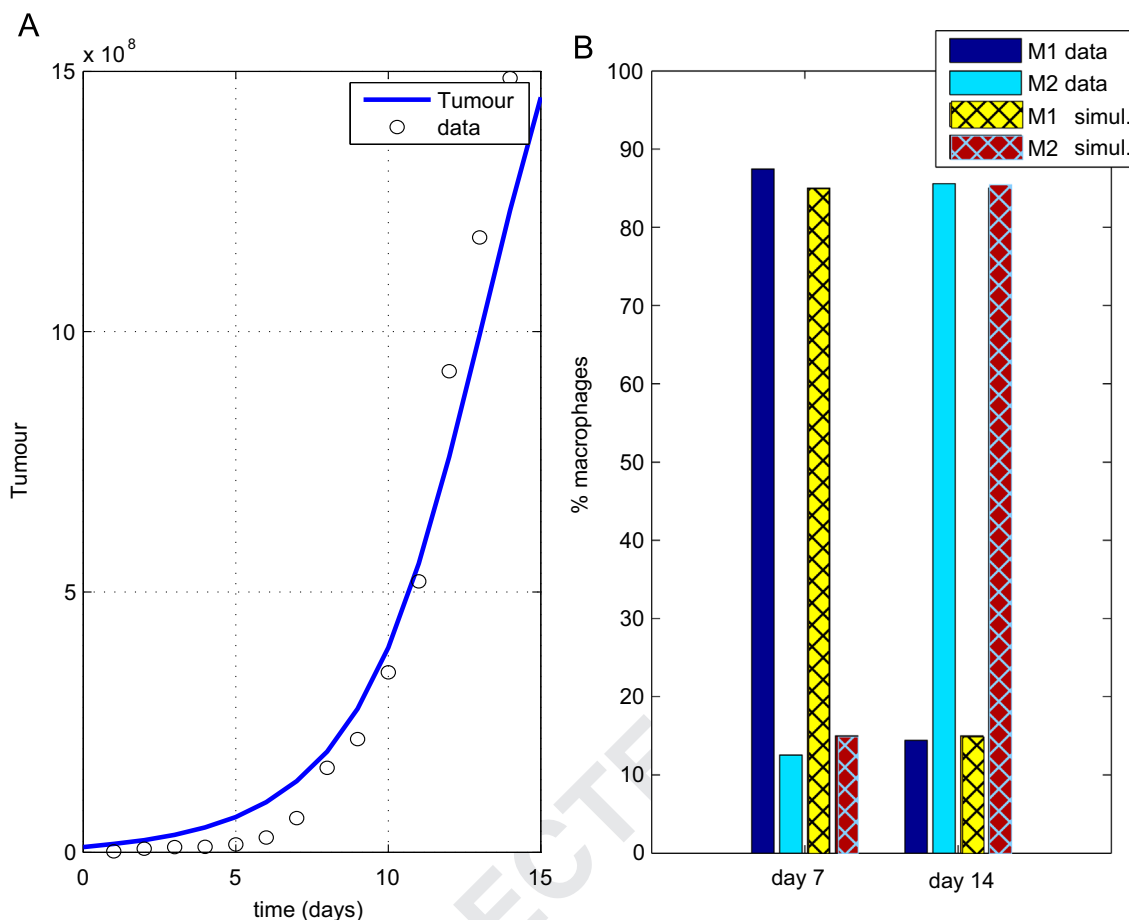


Fig. 2. (A) Numerical simulation of tumour growth in model Fig. 1 compared to data from Chen et al. (2011) for the melanoma growth in mice, and (B) the change in percentage of M1 and M2 macrophages at day 7 and day 14 for our numerical simulations and the experimental values shown in Chen et al. (2011).

analysis (where we change one value while keeping all other values fixed). This analysis also helps us identify the parameter space where we could see an improvement in cancer outcomes.

For the sensitivity analysis, we vary the initial conditions within the range shown in Table A4, the model parameters within the range shown in Table A6, and the ratio $k = k_{12}/k_{21}$ within the range shown in Table A3.

For each baseline value q of model parameters and initial conditions (that generated the simulations in Fig. 3 and which will be referred to as the *baseline model*), we consider the effect of changing q to $q + \Delta q$, where Δq is either positive or negative. In particular, if q is a parameter value, then q is changed with 7 incremental steps $\Delta q = 30\%q$ within the range $(-80\%q, +190\%q)$ (see Table A6). If q is an initial condition value, then q is changed with 6 incremental steps within the ranges shown in Table A4. Finally, if $q = k = k_{12}/k_{21}$, then we change k_{12} and k_{21} simultaneously from 4×10^{-7} to 4×10^{-3} in 100 steps creating 10,000 simulations. However, to keep the results tractable, in Table A3 we present the most informative 7-step changes in the ratio k , with $k_{12} \in (5 \times 10^{-5}, 2 \times 10^{-5})$ and $k_{21} \in (4 \times 10^{-5}, 1.6 \times 10^{-5})$.

The change from q to $q + \Delta q$ leads to a change in the total tumour size $x_T = x_{T_S} + x_{T_n}$ (see Fig. 4). Denoting by $X = x_T(20)$ the tumour size on day 20, as obtained with the baseline parameter values and initial conditions (see Fig. 3(A)), then the change in q leads to a change from X to $X + \Delta X$, where ΔX is the percentage change on day 20. We chose to focus on tumour size on day 20 since the experimental studies in Chen et al. (2011) show that the carrying capacity $\beta_T = 2 \times 10^9$ cells (corresponding to a tumour volume of $\approx 3 \text{ cm}^3$) is reached after 20 days. However, to ensure that the tumour is indeed at the carrying capacity and to

investigate long term prognosis, we also investigate the percentage change in tumour population on day 50.

Moreover, many experimental studies investigate the effect of the ratio M2/M1 on tumour size, to test whether this ratio can be used as a biomarker for tumour development (Herwig et al., 2013). Therefore, we will use sensitivity analysis to quantify the relationship between the ratio M2/M1 at day 7 (for comparison with the data; see Fig. 2) and the changes in the tumour population at days 20 and 50, as a result of varying k in the simulations.

While a decrease in the tumour might be the most desirable outcome, an increase in the number of days to reach a certain tumour size can extend the life expectancy. Therefore, we introduce a second value, Z , to represent the time the tumour grows to half the carrying capacity, i.e., to half the size obtained on day 20 with the baseline model (see Fig. 4). Thus, a change from q to $q + \Delta q$ will lead to a change from Z to $Z + \Delta Z$, which might not correlate with the change X to $X + \Delta X$ (as shown in Fig. 4). Note here that we refer to the growth until the tumour reaches half the carrying capacity as early tumour growth.

In the following subsections we show the change in the tumour size at days 20 and 50, and in the number of days to reach half the tumour size on day 20, when we vary the initial conditions (Section 5.1), the parameter values (Section 5.2), the ratio k (Section 5.3) and the ratio M2/M1 (Section 5.4).

5.1. Sensitivity to initial conditions

Fig. 5 shows that changing $x_{T_S}(0)$ (within the interval shown in Table A4) has the greatest effect on the final tumour population (panel A), and on the number of days to reach half of tumour size

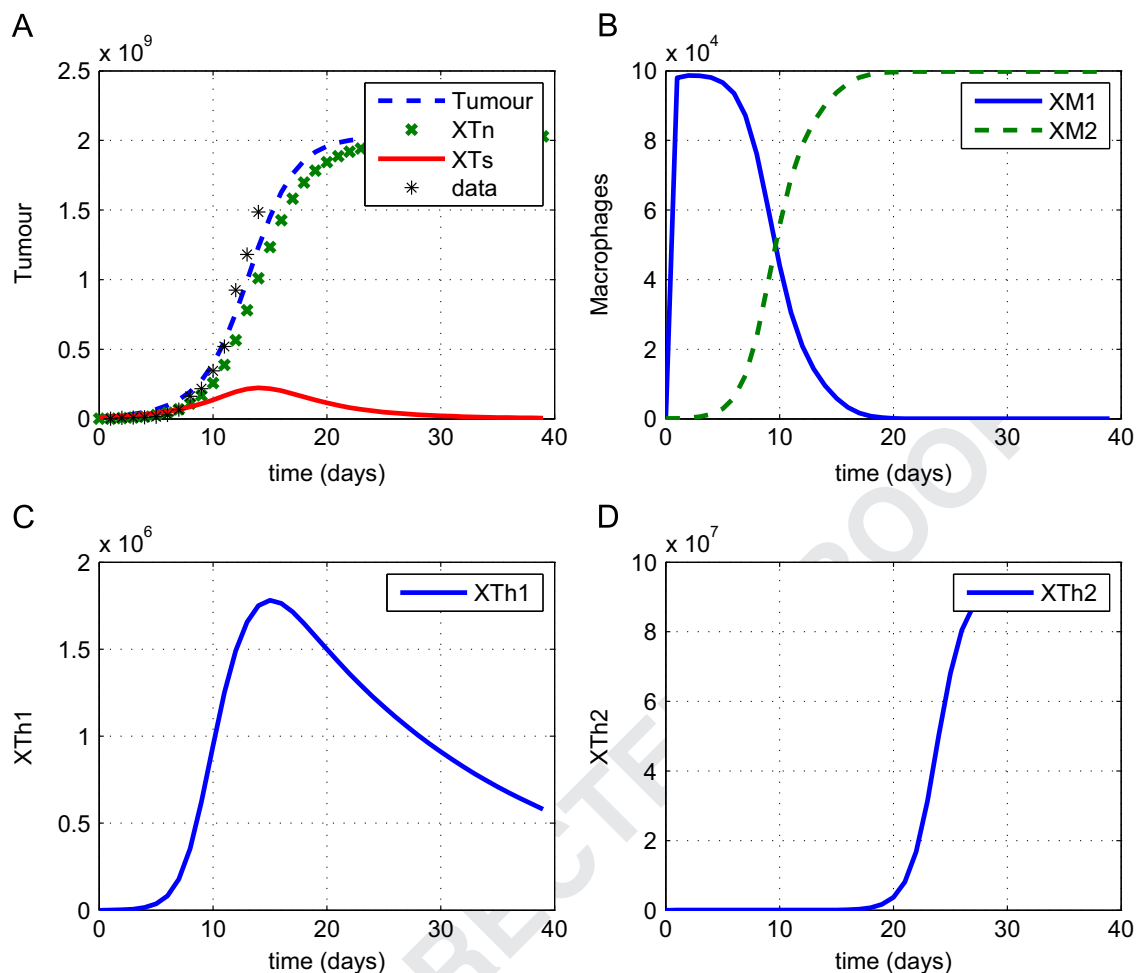


Fig. 3. Dynamics of tumour and immune cells, for the initial conditions and parameter values described in Tables A1 and A2. (A) Total number of tumour cells (dashed curve), x_{Tn} cells (crosses) and x_{Ts} cells (continuous curve). For comparison purposes, we also show tumour data from Chen et al. (2011); (B) x_{M1} and x_{M2} macrophages; (C) x_{Th1} cells; and (D) x_{Th2} cells.

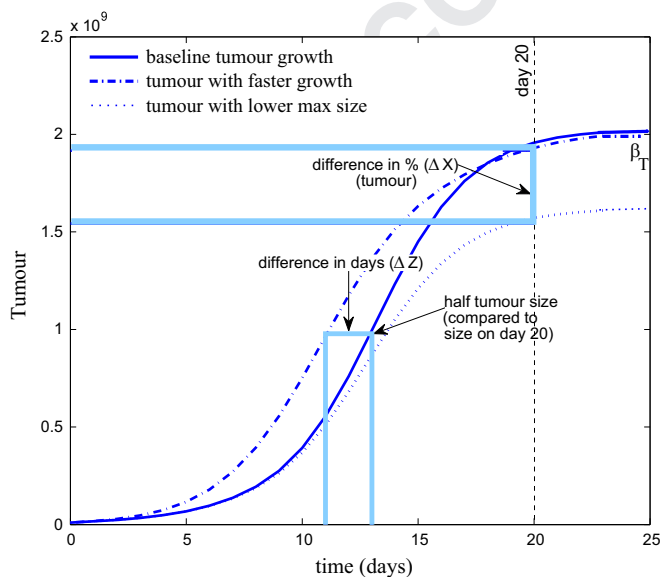


Fig. 4. Dynamics of tumour growth for the baseline model (continuous curve) and two simulations showing faster tumour growth (dash-dot curve) and tumour growth with smaller maximum size (dotted curve), to exemplify how we calculate ΔX and ΔZ . ΔX gives the percentage change in maximum tumour size, as model parameters are varied. ΔZ gives the change in the number of days until the tumour reaches half the size obtained with the baseline model on day 20.

on day 20 (panel B). A change in $x_{Tn}(0)$ (within the interval shown in Table A4) does not have a significant effect, which is not surprising since these cells can grow uncontrolled by the immune response. In regard to the change in the initial conditions for the immune cells, only a change in $x_{M2}(0)$ has some effect: (i) it can decrease the total tumour size by -3% or increase it by $+4\%$ (Table A4), or (ii) it can decrease/increase by ∓ 2 the number of days until the tumour reaches half the size obtained on day 20 with the baseline model (Table A5).

5.2. Sensitivity to parameters

Fig. 6 shows the effect that varying model parameters has on the percentage change in the tumour size (panel A; see also Table A6) and on the number of days to reach half the tumour size obtained on day 20 with the baseline model (panel B; see also Table A7). As expected, the proliferation rate r and the carrying capacity β_T have the largest influence on the tumour population. However, it is unexpected that the re-polarisation rates k_{12} and k_{21} for the M2 and M1 macrophages also have a large impact on tumour. These parameters appear in the steady states for x_{M1} and x_{M2} , and are involved in the ratio of M2/M1 macrophages. We will return to these rates in Section 5.3, when we will investigate in more detail the role of $k = k_{12}/k_{21}$ on tumour growth.

Other parameters that influence tumour dynamics are k_{sn} , the rate at which the x_{Ts} cells become x_{Tn} cells; δ_{mn} , the rate at which

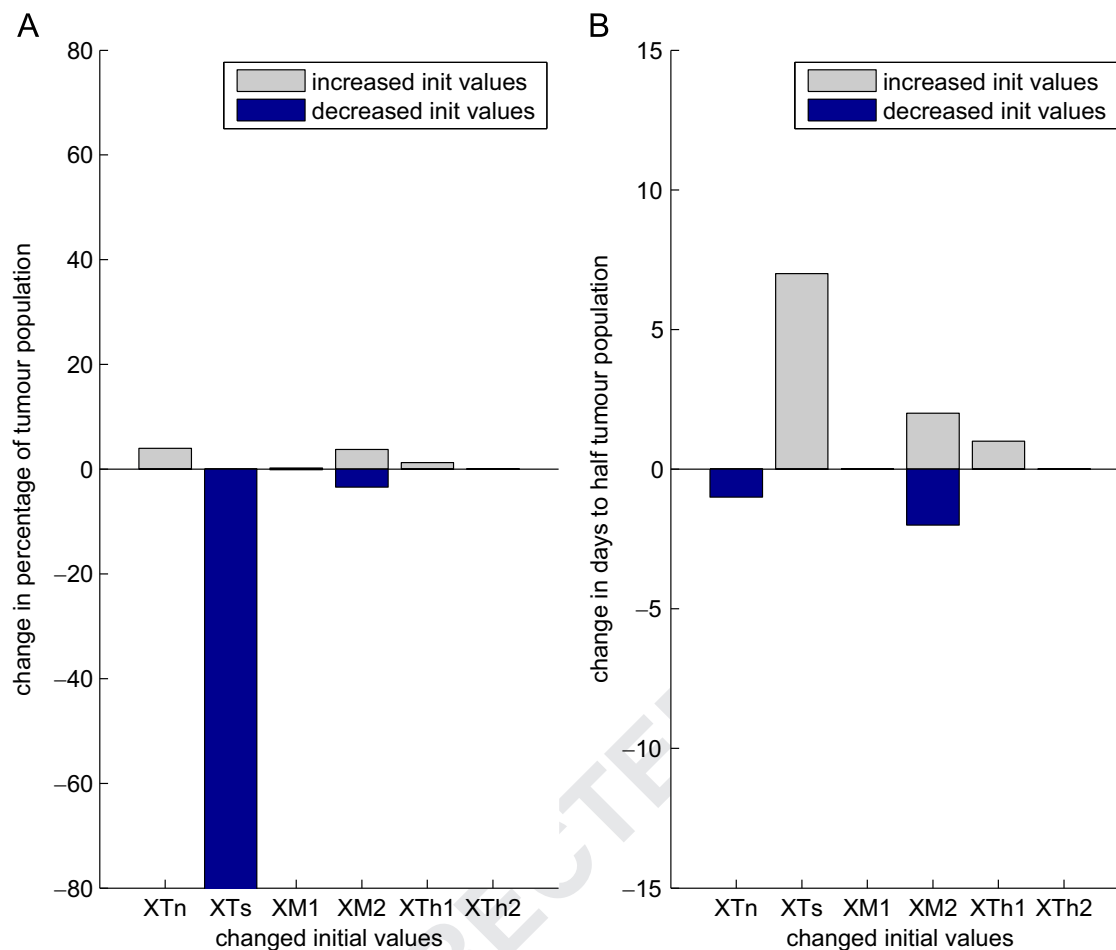


Fig. 5. Change in tumour as a result of variation in initial conditions from the baseline values, as described in Tables A4 and A5. (A) Percentage of change from the baseline tumour population after 20 days of simulation (Table A4) and (B) change in the number of days until the tumour reaches half the tumour size obtained in the baseline model on day 20 (Table A5).

x_{Tn} cells are eliminated by M1 macrophages; δ_{ms} , the elimination rate of x_{Ts} tumour cells by the M1 macrophages; δ_{m2} , the death rate of M2 cells. These results support the theory that both M1 and M2 cells influence tumour dynamics.

5.3. Sensitivity to the ratio $k = k_{12}/k_{21}$

In Fig. 7(A) we show the percentage change from the baseline model, in tumour size on day 20 versus the ratio $k = k_{12}/k_{21}$. For $k < 1$ the tumour is reduced by 40%, while for $k > 1$ the changes in tumour at day 20 can vary from -40% to $+5\%$, depending on the exact values of the rates k_{12} and k_{21} . In Fig. 7(B) we show the percentage change in tumour size on day 50 versus k . In this case, for $k \geq 1$ the tumours stay at their carrying capacity (i.e., no change from the value obtained with the baseline parameters). However, for $k < 1$, the tumour size on day 50 is reduced between 0 and 35%, again depending on the specific values of the macrophage repolarisation rates k_{12} and k_{21} . We deduce from here that the ratio $k = k_{12}/k_{21}$ is not a clear indicator of tumour dynamics; the particular values of k_{12} and k_{21} that lead to the same ratio k influence whether the tumour decreases or increases.

In Fig. 8 we plot the time-dynamics of tumour population $x_{Tn} + x_{Ts}$ for different values of k_{12} and k_{21} with the same ratio k ($k=3.3$ top panel; $k=1.2$ middle panel; $k=0.6$ bottom panel). The results clearly show that changing k_{12} and k_{21} while keeping $k = k_{12}/k_{21}$ constant leads to different medium-term ($0 < t < 25$) and long-term ($t > 35$) tumour dynamics.

To understand better the role of k_{12} and k_{21} rates on tumour dynamics, in Fig. 9 we graph the changes in tumour size and tumour growth versus the difference $k_{12} - k_{21}$. When $k_{12} - k_{21} \in (0, 1 \times 10^{-5})$, there is an abrupt shift for the percentage change in tumour size at day 20 (see Fig. 9(A)), leading to a reduction in tumour up to 42%. A similar shift, occurring for $k_{12} - k_{21} \in (-2 \times 10^{-5}, 0)$, can be observed also in the percentage change in tumour size at day 50 (see Fig. 9(B)), although this is accompanied by a smaller reduction in tumour.

5.4. Sensitivity to M2/M1 ratio

Changing the ratio $k = k_{12}/k_{21}$ also leads to a change in the ratio of M2 and M1 macrophages: x_{M2}/x_{M1} . In Fig. 10 we graph the time-dynamics of these macrophages for three different ratios of k ($k=3.3$ in top panel, $k=1.2$ in middle panel, $k=0.6$ in bottom panel). The dashed curves show the baseline dynamics of M1 macrophages and the crosses show the baseline dynamics of M2 macrophages (for the baseline k_{12} and k_{21} values; as in Fig. 3). The dashed-dotted and continuum curves show the dynamics of M1 and M2 macrophages, respectively, for various k_{12} and k_{21} values that lead to specific k ratios. In none of these cases is the tumour completely eliminated; however the final tumour sizes approach different steady-state values (as shown in Fig. 8). This analysis indicates that the same ratio k can produce different M2/M1 profiles, with the shift between type-I and type-II immune responses occurring at different days. The change in the tumour

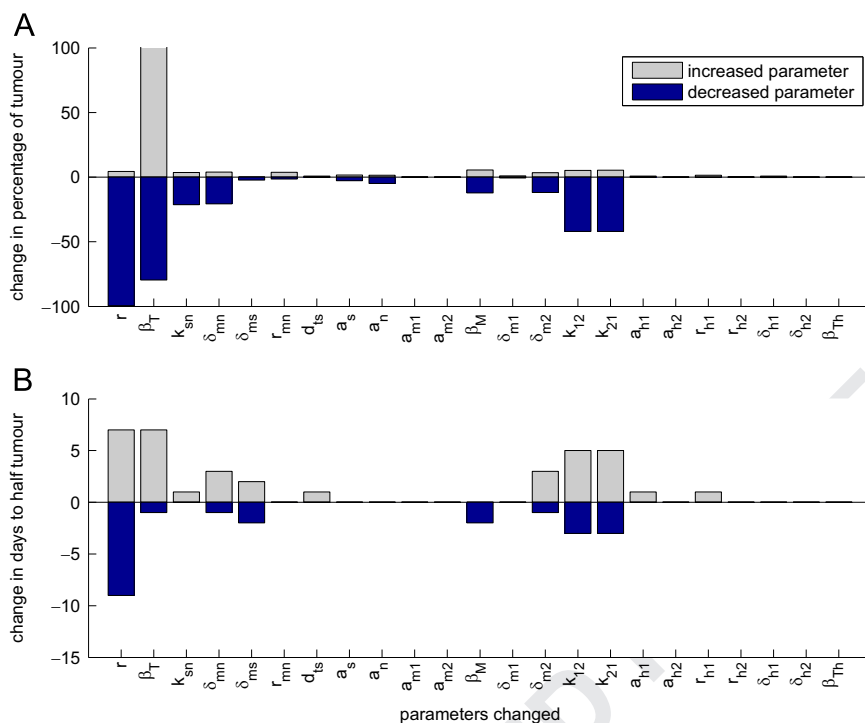


Fig. 6. Change in tumour size, from the baseline model, as a result of the change in model parameters from -80% to $+190\%$ of their baseline values (shown in Tables A6 and A7). (A) Percentage change of tumour size on day 20 (Table A6) and (B) change in the number of days until tumour reaches half the tumour size observed on day 20 with the baseline model (Table A7).

dynamics is related to the day when the M2 cells outnumber the M1 cells.

In Fig. 11 we show the ratio M2:M1 at days 7 and 14 (i.e., $x_{M2}(7)/x_{M1}(7)$ and $x_{M2}(14)/x_{M1}(14)$) for different k values. For $k < 1.2$ the dynamics on days 7 and 14 is dominated by the M1 macrophages. For $k > 1.2$, the dynamics on days 7 and 14 is dominated by the M2 macrophages. For $k = 1.2$ (see the plots on the main diagonal), there are different percentages of M2 and M1 macrophages on day 7 and day 14, depending on the particular values of k_{12} and k_{21} used.

In Fig. 12 we show the change in tumour size on day 20 (panel A) and day 50 (panel B), as we vary k_{12} and k_{21} within the range shown in Table A3, which then leads to a change in x_{M2}/x_{M1} at day 7. The results show that the tumour sizes on day 20 corresponding to $x_{M2}(7)/x_{M1}(7) \leq 1$ are completely different from the tumour sizes corresponding to $x_{M2}(7)/x_{M1}(7) > 1$. Note here the lower median value for tumour size when $x_{M2}/x_{M1} \leq 1$ compared to the case $x_{M2}/x_{M1} > 1$. These results persist also for the tumour sizes calculated at day 50, however, in this case the median value for tumour size when $x_{M2}/x_{M1} \leq 1$ is slightly higher. This is consistent with the experimental results by Herwig et al. (2013), who classified melanoma in 2 different classes of tumour gene expression profiles based on the M2/M1 ratio (for a group of 20 patients).

6. Summary and discussion

The role of M1 and M2 macrophages on tumour growth, and the use of M2/M1 ratio as an early-time marker for tumour prognosis, has attracted lots of interest over the last few years. Despite numerous experimental studies on the topic, we still lack a deeper understanding of the dynamics between the M1 and M2 macrophages and the tumour environment.

In this paper, we introduced a mathematical model that investigated the dynamics between the M1 and M2 macrophages, Th1 and Th2 immune cells, immunogenic and non-immunogenic

tumour cells. We first focused on the steady states exhibited by this model and their stability. The results indicated that, when the tumour and immune cells were present, the steady states were not unique (see also Fig. B1(B)). The existence of multiple states emphasised the complexity of the model dynamics, and the difficulty to understand analytically the role of the M2:M1 ratio on tumour persistence/elimination. Then, we performed an in-depth local sensitivity analysis to investigate the role of model parameters and of initial conditions on tumour outcome. Particular attention was paid to the role of $k = k_{12}/k_{21}$ on the shift from a type-I immune response to a type-II immune response.

The sensitivity analysis allowed us to identify the parameter values that can lead to a slow-down in tumour growth or to smaller tumour sizes. In addition to the expected importance of tumour growth rate r and tumour carrying capacity β_T on overall tumour dynamics, two other parameters, k_{12} and k_{21} , showed unexpected impact on tumour growth and decay (see Figs. 6 and 10). Moreover, we showed that while the ratio $k = k_{12}/k_{21}$ is important in predicting long-term tumour control or growth to the carrying capacity, the exact tumour sizes are given by the particular values of the re-polarisation rates k_{12} and k_{21} (Figs. 7–10). In addition, the rates k_{12} and k_{21} influenced the day of the shift from a type-I to a type-II immune response (and subsequent tumour growth); see Fig. 10.

The results in Figs. 9 and 12 also suggested that an early-time ratio of M2 : M1 < 1 cannot predict the long-term tumour progression (see Fig. 12). Unfortunately, there are not many experimental studies that track the time-changes of M2:M1 ratio, which can be used for comparison with our numerical results. Among the very few existent studies, the one in Chen et al. (2011) showed a change from an early-time ratio of M2 : M1 < 1 to a long-term ratio of M2 : M1 > 1 that was associated with tumour growth (see also Fig. 2). Therefore, more experimental studies are necessary to validate the hypotheses proposed by this theoretical model.

We emphasise that the results of our study were based on available data from mice experiments. However, even if mouse

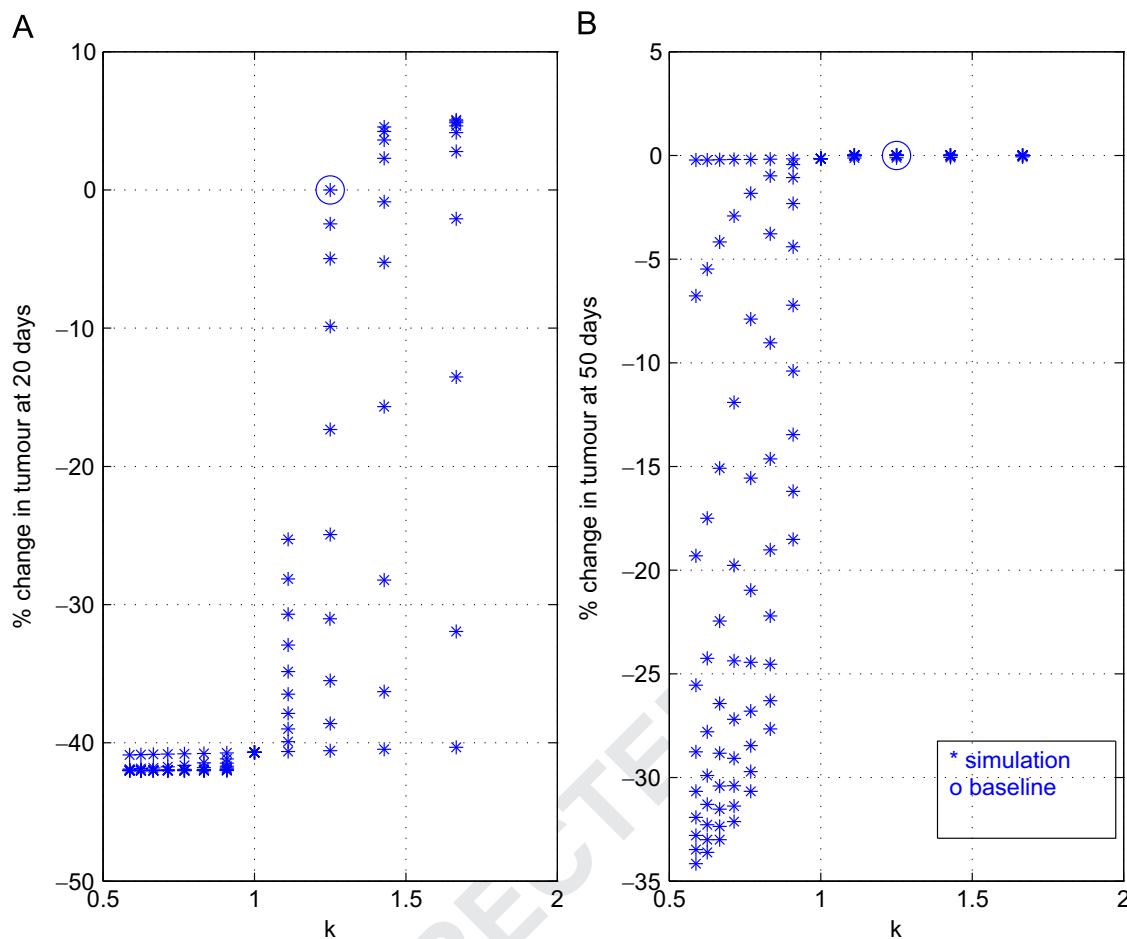


Fig. 7. Percentage change from the baseline model (see the open circle for $k=1.2$) in: (A) tumour cells on day 20, and (B) tumour cells on day 50, for different values of the ratio $k = k_{12}/k_{21}$ (as given by Table A3). (A) For $k > 1$, tumour size on day 20 can increase or decrease depending on the actual values of k_{12} and k_{21} . For $k < 1$, tumour size on day 20 always decreases. (B) For $k > 1$, the tumours always reach the carrying capacity on day 50. For $k < 1$ the tumours can be reduced in size by varying degrees, depending on the actual values of k_{12} and k_{21} .

models have been used widely to study the interactions between the immune system and cancer to propose hypotheses in regard to human cancers, it is possible that data from human clinical trials (still scarce at this moment) would lead to different results. Nevertheless, it was not the goal of our study to compare the results for mouse and human data sets. Rather, our study focused on investigating the role of ratio of M1 and M2 macrophages as a marker for tumour prognosis in mouse models. As mentioned before, we showed that the ratio of mouse macrophage populations can be a suitable predictor of tumour outcome if $x_{M2}/x_{M1} > 1$ in early tumour stages, i.e., before the tumour reaches half the carrying capacity (in Fig. 12 we focused on the value of this ratio at day 7). If these results can be confirmed also for human data, then they can have implications to human treatment protocols, since clinicians could use the ratio $x_{M2}/x_{M1} > 1$ as a biomarker for decisions regarding various long-term patient treatments. Moreover, the possibility of re-programming the environment towards a M1 phenotype (as suggested, for example, by Heusinkveld and van der Burg, 2011; Tang et al., 2013) could also impact positively the outcome of cancer treatments, by creating the possibility of a reduced long-term tumour burden that can be further reduced with other types of treatment (e.g., combinations of immune therapies, viral therapies and/or chemotherapies).

To understand better the molecular-level mechanisms that control the dynamics of M1 and M2 cells, and their interactions with the tumour cells (with the purpose of designing treatments that would re-program the M2 macrophages to a M1-phenotype)

it is necessary to add more detail to the model (1). Further investigation should focus on the role of molecular-level dynamics (i.e., the pro- and anti-tumour cytokines produced by both Th cells and macrophages) on the pro-tumour and anti-tumour immune responses.

Finally, we stress that the model introduced in this paper has a number of limitations. First, as mentioned before, the results of the model are valid only for mouse data. While it would be interesting to parametrise the model also for human data (to test the validity of these results in the context of human clinical trials), such an investigation is beyond the scope of the current study. Second, we focused only on the non-spatial dynamics of tumour and immune cells. However, tumours are highly heterogeneous and the immune cells might be localised in particular regions of the tumour. For example, the tumour-associated macrophages are usually found in the perivascular and cortical regions of the tumour, where they contribute to tumour growth and invasion (Carmona-Fontaine et al., 2013). In general, the mechanisms of immune cells localisations in particular areas of the tumours are still quite poorly understood, and future studies are necessary to understand the potential for new therapeutic avenues based on influencing this spatial localisation of immune cells. Last but not the least, the complex interactions between the tumour and immune cells give rise to highly nonlinear dynamics, which cannot be fully understood only via steady-state analysis, numerical simulations and sensitivity analysis. Nonlinear analysis and

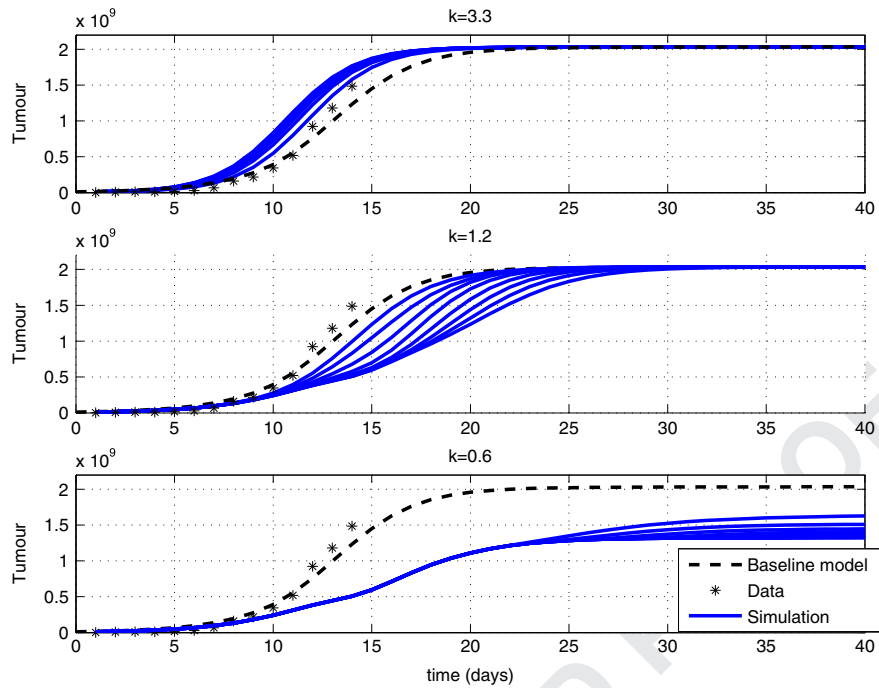


Fig. 8. Change in tumour population, from the baseline model, as a result of the change in the ratio $k = k_{12}/k_{21}$. Simulations are performed by changing the values k_{12} and k_{21} for different ratios k ($k=3.3$, $k=0.6$, and the baseline value $k=1.2$). Since different combinations of k_{12} and k_{21} result in the same ratio but with different tumour dynamics, it implies that the ratio k cannot be used to predict the tumour dynamics.

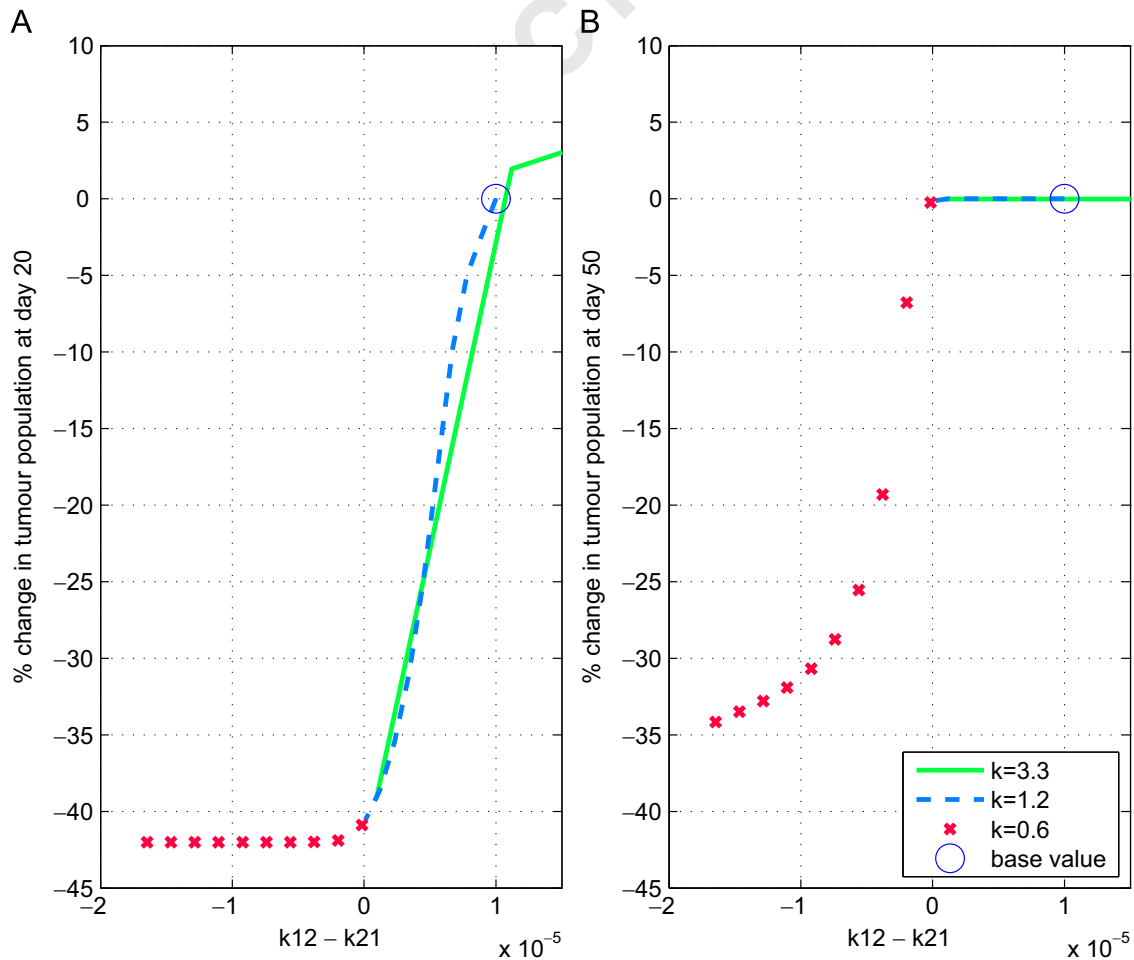


Fig. 9. Percentage of change, from baseline value (open circle), in tumour size on day 20 (panel A) and on day 50 (panel B) when $k_{12} - k_{21}$ is varied while keeping constant the ratio $k = k_{12}/k_{21}$ ($k=3.3$: continuous curve; $k=1.2$: dashed curve; $k=0.6$: asterisk).

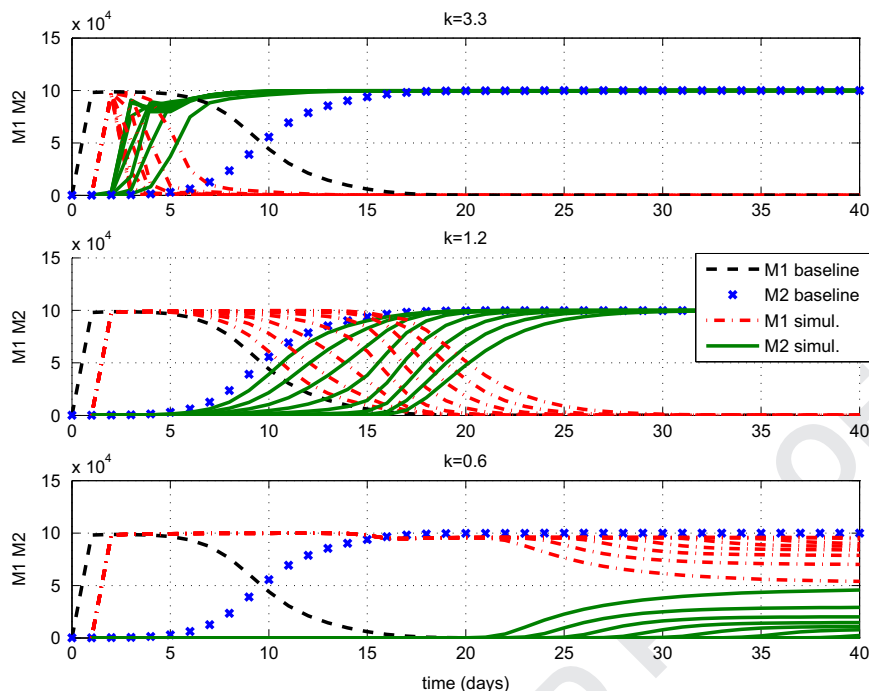


Fig. 10. Time-dynamics of M1 and M2 macrophages for different values of $k = k_{12}/k_{21}$: $k=3.3$, $k=1.2$ (baseline ratio), and $k=0.6$. In addition to showing the baseline dynamics of M1 and M2 macrophages, we also run simulations with multiple k_{12} and k_{21} values resulting in the same ratio. For $k > 1$ the M2 macrophages dominate the dynamics, and the tumour reaches the carrying capacity (see also Fig. 8 top two panels). For $k=0.6$ the M1 macrophages dominate the dynamics, and the tumour is reduced below the carrying capacity (see also Fig. 8 bottom panel).

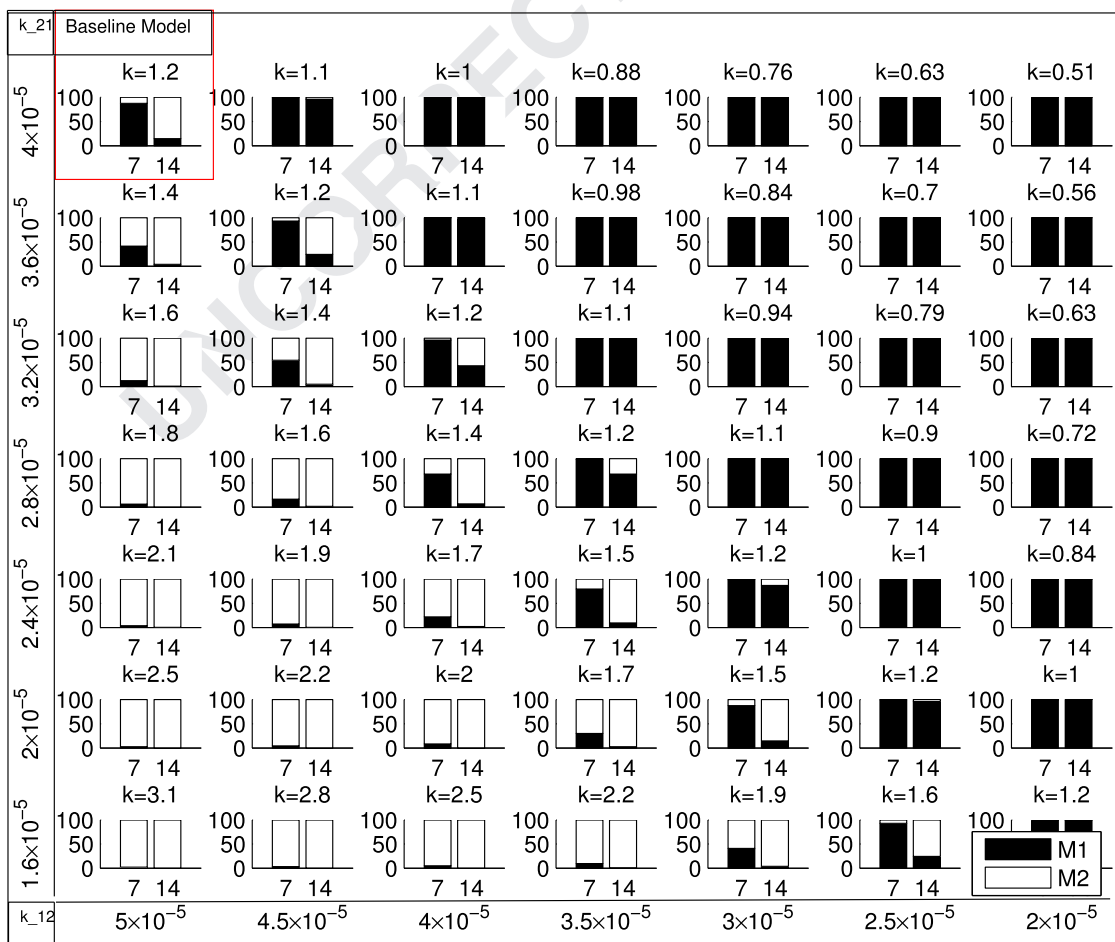


Fig. 11. The percentage of M2 and M1 macrophages on days 7 and 14, for different ratios of $k = k_{12}/k_{21}$. The ratio is shown above each small figure. Simulations are performed by changing k_{21} from 4×10^{-5} to 1.6×10^{-5} (see vertical axis) and k_{12} from 5×10^{-5} to 2×10^{-5} (see horizontal axis) in 7 steps.

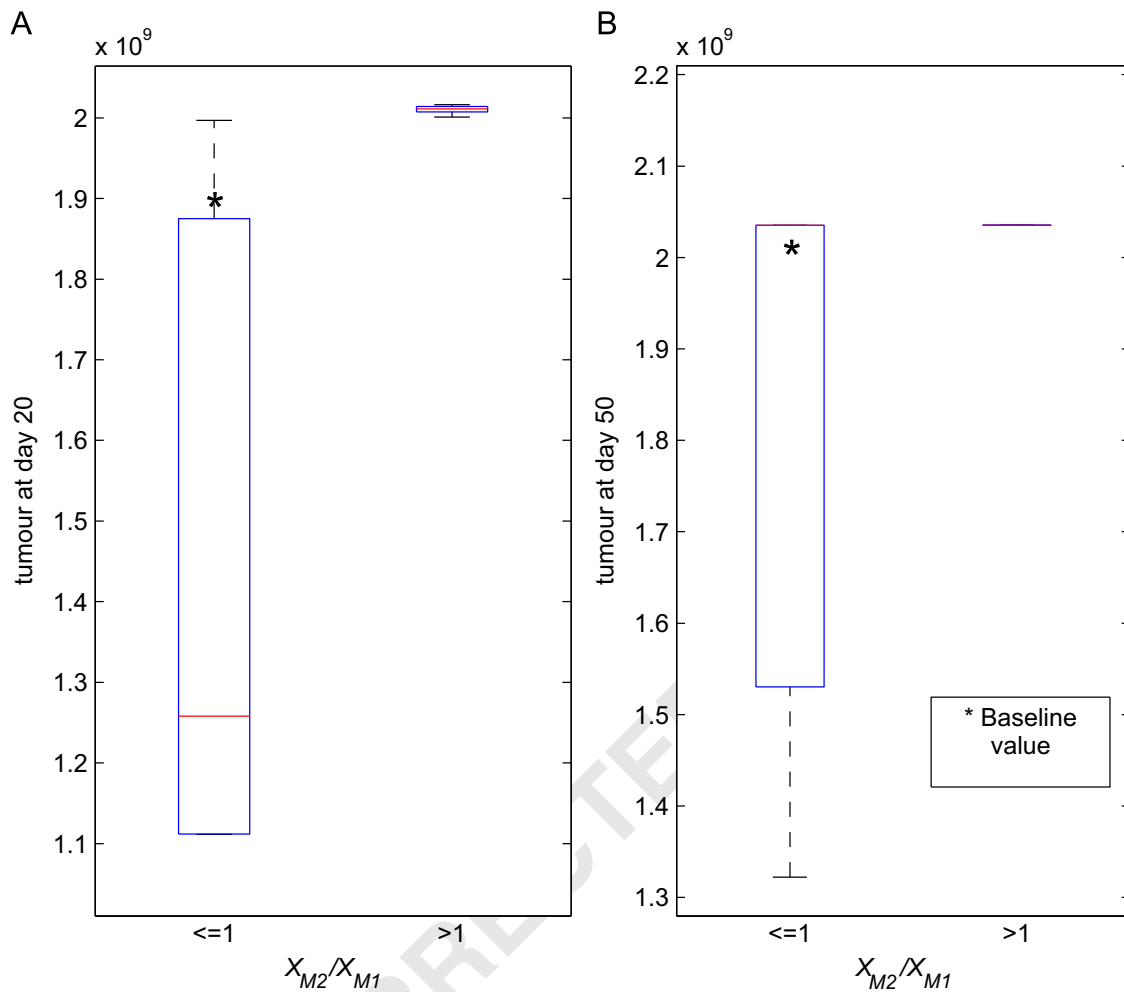


Fig. 12. (A) Total tumour size on day 20, when the ratio of M2/M1 macrophages on day 7 is either $x_{M2(7)}/x_{M1(7)} > 1$ or $x_{M2(7)}/x_{M1(7)} \leq 1$, as a result of varying $k_{21} \in (1.6 \times 10^{-5}, 4 \times 10^{-5})$ and $k_{12} \in (2 \times 10^{-5}, 5 \times 10^{-5})$ in 7 steps. (B) Total tumour size on day 50, for $x_{M2(7)}/x_{M1(7)} > 1$ and $x_{M2(7)}/x_{M1(7)} \leq 1$, as a result of varying $k_{21} \in (1.6 \times 10^{-5}, 4 \times 10^{-5})$ and $k_{12} \in (2 \times 10^{-5}, 5 \times 10^{-5})$ in 7 steps.

bifurcation theory should be used in the future to shed light on the observed dynamics.

Acknowledgements

N.dB. acknowledges support from the BIOMICS project (EU FP7 Grant no. 318202). R.E. acknowledges support from an Engineering and Physical Sciences Research Council (UK) Grant no. EP/K033689/1 and a Northern Research Partnership (Scotland) grant.

Appendix A. Summary of model parameters and variables

Table A1 summarises the variables used in model (1), together with their initial values (i.e., the initial conditions for the simulations) and the ranges within which we varied these initial values for the local sensitivity analysis. Table A2 summarises the parameters used throughout this paper, along with their values and units. Next, we describe how we estimated some of the parameters in Table A2.

A.1. Parameter estimation

- To approximate the tumour growth rate r , we fit Eq. (1a) with no immune response to the melanoma growth data from Chen

Table A1

Summary of variables used in the model, the baseline initial conditions (IC) and the range of IC used for the local sensitivity analysis.

States	Description	Baseline IC	Range IC
x_{Tn}	Density of non-immunogenic tumour cells	10^3	$(1, 10^7)$
x_{Ts}	Density of immunogenic tumour cells	10^6	$(1, 10^7)$
x_{M1}	Density of M1 macrophages	100	$(10, 10^4)$
x_{M2}	Density of M2 macrophages	100	$(10, 10^4)$
x_{Th1}	Density of Th1 helper cells	0	$(0, 10^5)$
x_{Th2}	Density of Th2 helper cells	0	$(0, 10^5)$

et al. (2011). We thus obtain $r = 0.565$ cells/day, in line with the values reported by Eikenberry et al. (2009) (see Fig. 2(A)).

- Most experimental studies euthanise the mice when the tumour reaches 2–3 cm^3 . In Chen et al. (2011), the tumour reached a volume of $\approx 3 \text{ cm}^3$ on day 14. Therefore, we choose the carrying capacity for the tumour to be $\beta_T = 2 \times 10^9$ (on the same order of magnitude as other theoretical studies; see Eftimie et al., 2010).
- To calculate the death rate δ_x of various cells, we use the formula $t_{1/2} = \ln(2)/\delta_x$, where $t_{1/2}$ is their half-life. The half-life of mouse circulating blood monocytes, the precursor of macrophages, varies from about 17.4 h (Van Furth, 1989; Kuroda, 2010) to 5 days (Ginhoux and Jung, 2014). For macrophages, we assume an average half-life of 3 days and calculate $\delta_{m1,m2} = \ln(2)/3 \approx 0.23$ (similar to

Table A2

Summary and description of parameters that appear in model (1). Parameters are estimated by fitting model (1) to the experimental data from Chen et al. (2011) and data from other experimental papers – as described in the *Parameter estimation* section in Appendix A.1, or they are sourced directly from the existent mathematical literature – indicated by a “*”.

Param.	Value	Units	Description	Reference
r	0.565	day ⁻¹	Proliferation rate of tumour cells	Chen et al., 2011
β_T	2×10^9	cells	Carrying capacity of tumour cells	Chen et al. (2011)
k_{sn}	0.1	day ⁻¹	Rate at which x_{Ts} become x_{Tn}	Guess
δ_{mn}	2×10^{-6}	(day cells) ⁻¹	Killing rate of x_{Tn} by x_{M1}	Baba et al. (2008)
δ_{ms}	2×10^{-6}	(day cells) ⁻¹	Killing rate of x_{Ts} by x_{M1}	Baba et al. (2008)
r_{mn}	1×10^{-7}	(day cells) ⁻¹	Proliferation rate of x_{Tn} cells in the presence of x_{M2} cells	Guess
δ_{ts}	5.3×10^{-8}	(day cells) ⁻¹	Killing rate of x_{Ts} by x_{Th1}	Hung et al. (1998)
a_s	1×10^{-6}	(day cells) ⁻¹	Activation rate of x_{M1} triggered by x_{Ts} antigens	Guess
a_n	5×10^{-8}	(day cells) ⁻¹	Activation rate of x_{M2} mediated by cytokines and growth factors produced by x_{Tn}	Guess
a_{m1}	5×10^{-8}	(day cells) ⁻¹	Activation rate of x_{M1} by type-I cytokines produced by x_{Th1}	Guess
a_{m2}	5×10^{-8}	(day cells) ⁻¹	Activation rate of x_{M2} by type-II cytokines produced by x_{Th2}	Guess
β_M	1×10^5	cells	Carrying capacity of M1,M2 cells	Guess
δ_{m1}	0.2	day ⁻¹	Death rate of x_{M1} cells	Wang et al. (2012)*
δ_{m2}	0.2	day ⁻¹	Death rate of x_{M2} cells	Wang et al. (2012)*
k_{12}	5×10^{-5}	(day cells) ⁻¹	Rate at which x_{M1} become x_{M2}	Chen et al. (2011)
k_{21}	4×10^{-5}	(day cells) ⁻¹	Rate at which x_{M2} become x_{M1}	Chen et al. (2011)
a_{h1}	8×10^{-3}	day ⁻¹	Activation rate of x_{Th1} by type-I cytokines produced by x_{M1}	Ribeiro et al. (2002)*
a_{h2}	8×10^{-3}	day ⁻¹	Activation rate of x_{Th2} by type-II cytokines produced by x_{M2}	Ribeiro et al. (2002)*
r_{h1}	9×10^{-6}	(day cells) ⁻¹	Proliferation rate of x_{Th1} in the presence of type-I cytokines produced by x_{M1} cells	Guess
r_{h2}	9×10^{-6}	(day cells) ⁻¹	Proliferation rate of x_{Th2} in the presence of type-II cytokines produced by x_{M2} cells	Guess
δ_{h1}	0.05	day ⁻¹	Natural death rate of x_{Th1} cells	Pepper and Jenkins (2011)
δ_{h2}	0.05	day ⁻¹	Natural death rate of x_{Th2} cells	Pepper and Jenkins (2011)
β_{Th}	1×10^8	cells	Carrying capacity of Th cells	Guess

the value in Wang et al., 2012). In regard to the effector CD4⁺ T cells, about 90% of cells dies within the 7–14 days of the contraction phase (Pepper and Jenkins, 2011). Therefore we calculate $\delta_{h1,h2} \in (\ln(2)/14, \ln(2)/7) \approx (0.049, 0.099)$. Throughout this paper, we choose $\delta_{h1,h2} = 0.05$.

- Experimental results in Chen et al. (2011) have shown that on day 7 there were only 15% M2 macrophages, while on day 14 this percentage increased to 85% M2 macrophages. We use these values to fit k_{12} , the rate at which M1 macrophages become M2, and k_{21} , the rate at which M2 macrophages become M1 (see Fig. 2C), r_{mn} the proliferation rate of x_{Tn} cells in the presence of M2 macrophages, and β_M the carrying capacity of macrophages.
- The metastatic mouse melanoma tumour cells have a very high mutation rate compared to other tumour lines (Cillo et al., 1987). For example, the B16F10 melanoma cells have a rate of generation of drug-resistant clones of at least 10^{-5} /cell/generation (Cillo et al., 1987; Hill et al., 1984), while lower metastatic tumours can have a mutation rate of $\approx 10^{-7}$ /cell/generation (Mareel et al., 1991). To model these high melanoma mutation rates, we assume an average growing cell population of $\approx 10^4$ cells/generation, a 1-day generation of cells (since the doubling time is about 1.2 days), and take the mutation rate $k_{sn} = 10^{-5}$ /cell/day $\times 10^4$ cells = 0.1/day.
- To approximate the maximum rate at which the effector cells kill the tumour cells (at an effector:target ratio of 1:1), we use the following formula (where we ignore the proliferation of tumour cells, since we assume that cells do not proliferate anymore in vitro):

$$\frac{dT}{dt} = -\delta_{kill}TE, \quad (A.1)$$

with T describing the target cells ($T = x_{Tn}$ or $T = x_{Ts}$) and E describing the effector cells ($E = x_{M1}$ or $E = x_{Th1}$). To approximate δ_{kill} for macrophages (i.e., $\delta_{kill} = \delta_{ms} = \delta_{mn}$), we note that Baba et al. (2008) incubated for 18 h CD4⁺CD8⁺ macrophages of M1 phenotype with four different tumour cell lines. The killing of tumour cells reached maximum rate at an effector:target ratio of 30:1 (i.e., 1.2×10^6 effector cells and 4×10^4 target cells). Moreover, the percent specific lysis varied between

10% and 97%. Integrating Eq. (A.1) with respect to time from $t=0$ hrs to $t_i = 18$ h, replacing E with $E=30T$ (for an effector:target ratio of 30), and assuming that the total number of target cells at the end of the incubation time t_i is $T(t_i) = 100 - \%Lysis$, we obtain

$$\delta_{kill} = \frac{\%Lysis}{T(0)(100 - \%Lysis)30t_i}. \quad (A.2)$$

Therefore, for $t_i = 18$ h = 0.75 days and $T(0) = 4 \times 10^4$ cells, we obtain

$$\delta_{kill} = 3.6 \times 10^{-5}, \quad \text{for } \%Lysis = 97\%, \quad (A.3)$$

$$\delta_{kill} = 1.2 \times 10^{-7}, \quad \text{for } \%Lysis = 10\%. \quad (A.4)$$

For the purpose of this paper, we will consider $\delta_{mn} = \delta_{ms} = 2 \times 10^{-6}$, corresponding to an average tumour %Lysis = 65%.

Finally, to approximate δ_{kill} for Th1 cells (i.e., $\delta_{kill} = \delta_{ts}$), we note that (Hung et al., 1998) incubated 10^6 B16 tumour cells with CD4 T cells. The maximum %Lysis was 30%, and was obtained at an effector:target ratio of about 32:1. Using again (A.1), and the assumption that cells were incubated for about 6 h (=0.25 days), we obtain a killing rate

$$\delta_{kill} = \delta_{ts} = 5.3 \times 10^{-8}. \quad (A.5)$$

Next, we introduce Tables A3–A7 that contain the values of parameters and initial conditions used for the sensitivity analysis in Section 5.

Appendix B. Number of steady states

To investigate the number of TF1P states, we substitute x_{Th1}^* given by (2) into the expression for x_{M1}^* (given by the same equation), which leads to

$$A_1(x_{Th1}^*)^3 + B_1(x_{Th1}^*)^2 + C_1(x_{Th1}^*) + D_1 = 0, \quad (B.1)$$

Table A3

Changes in the ratio $k = k_{12}/k_{21}$ for the sensitivity analysis. k_{12} is changed from 5×10^{-5} to 2×10^{-5} , and k_{21} is changed from 4×10^{-5} to 1.6×10^{-5} in 7 steps.

k_{21}	k	k	k	k	k	k	k
4×10^{-5}	1.2	1.1	1	0.88	0.75	0.63	0.51
3.6×10^{-5}	1.4	1.2	1.1	0.98	0.84	0.7	0.56
3.2×10^{-5}	1.6	1.4	1.2	1.1	0.94	0.79	0.63
2.8×10^{-5}	1.8	1.6	1.4	1.2	1.1	0.9	0.72
2.4×10^{-5}	2.1	1.9	1.7	1.5	1.2	1	0.84
2×10^{-5}	2.5	2.2	2	1.7	1.5	1.2	1
1.6×10^{-5}	3.1	2.8	2.5	2.2	1.9	1.6	1.2
k_{12}	5×10^{-5}	4.5×10^{-5}	4×10^{-5}	3.5×10^{-5}	3×10^{-5}	2.5×10^{-5}	2×10^{-5}

Table A4

Percentage change in tumour size on day 20 (columns 4 and 6), for simulations with different initial conditions (IC). Columns 1 and 2 show, respectively, the baseline values for the IC and the range within which they are varied. Columns 3 and 5 show the initial conditions that lead to a maximum decrease/increase in tumour size on day 20.

IC baseline value	Range for IC	IC for max tumour decrease	Max % decrease in tumour	IC for max tumour increase	Max % increase in tumour
$x_{Tn}(0) = 10^3$	$(1, 10^7)$	1	0	10^7	4
$x_{Ts}(0) = 10^6$	$(1, 10^7)$	1	-98	10^7	0
$x_{M1}(0) = 10^2$	$(10, 10^4)$	10	0	10^4	0
$x_{M2}(0) = 10^2$	$(10, 10^4)$	10	-3	10^4	4
$x_{Th1}(0) = 0$	$(0, 10^5)$	0	0	3×10^4	1
$x_{Th2}(0) = 0$	$(0, 10^5)$	0	0	10^5	0

Table A5

Maximum increase/decrease in the number of days to reach half the tumour population obtained on day 20 with the baseline model (see also Fig. 4), as we vary the initial conditions (IC). Columns 1 and 2 show, respectively, the baseline values for the IC and the range within which they are varied. Columns 3 and 5 show the initial conditions that lead to a maximum decrease/increase in the number of days to reach half the tumour population on day 20.

Baseline IC value	Range for IC	IC for max time decrease	Max decrease in nbr. days	IC for max time increase	Max increase in nbr. days
$x_{Tn} = 10^3$	$(1, 10^7)$	5×10^6	-1	1	0
$x_{Ts} = 10^6$	$(1, 10^7)$	10^7	0	1	7
$x_{M1} = 100$	$(10, 10^4)$	10	0	10	0
$x_{M2} = 100$	$(10, 10^4)$	5010	-2	10	2
$x_{Th1} = 0$	$(0, 10^5)$	0	0	10^4	0
$x_{Th2} = 0$	$(0, 10^5)$	0	0	0	0

where

$$A_1 = -\frac{a_{m1}r_{h1}\beta_M}{\beta_{Th}}, \quad B_1 = a_{m1}\beta_M r_{h1} - a_{m1}\delta_{h1} + \frac{\delta_{m1}\beta_M r_{h1}}{\beta_{Th}}, \quad (B.2a)$$

$$C_1 = a_{m1}\beta_M a_{h1} - \delta_{m1}\beta_M r_{h1}, \quad D_1 = -\delta_{m1}\beta_M a_{h1}. \quad (B.2b)$$

This equation has a unique real solution (for the parameter values given in Table A2), and hence there is a unique TF1IP steady state.

Similarly, we can investigate the number of TF2IP states by substituting x_{Th2}^* given by (3) into the expression for x_{M2}^* (also given by (3)), which leads to a cubic equation similar to (B.1). Since this cubic equation has a unique solution, we deduce that also the TF2IP state is unique.

Due to the complexity of the TFIP states, we can investigate their uniqueness only numerically. In Fig. B1(A) we show that the solution curves of (4) intersect for an infinite number of values, and thus system (1) can have an infinite number of steady states.

To investigate the number of TP1IP states, note that in (5) neither x_{M1}^* nor x_{Th}^* are affected by x_{Tn}^* (x_{M1}^* is influenced only by $x_{Ts}^* = 0$). Thus the states x_{M1}^* and x_{Th1}^* in (5) are also solutions of Eq.

(B.1), and they are unique. Similarly, the TP2IP state is unique (which can be checked easily by substituting (6b) into (6a)). As discussed in Appendix C, this state is stable.

Finally, the number of TPIP states is investigated graphically in Fig. B1(B). Note that the surface curves given by the right-hand side of Eqs. (1a), (1c) and (1d) (obtained after we substitute into these equations the values of x_{M1}^* and x_{M2}^* calculated from (1e) and (1f)) intersect for an infinite number of x_{Tn}^* values. Therefore, there is an infinite number of TPIP states.

Appendix C. Jacobian matrix

The Jacobian matrix associated with system (1) is given by:

$$J = \begin{pmatrix} a_{11} & a_{12} & a_{13} & a_{14} & a_{15} & a_{16} \\ a_{21} & a_{22} & a_{23} & a_{24} & a_{25} & a_{26} \\ a_{31} & a_{32} & a_{33} & a_{34} & a_{35} & a_{36} \\ a_{41} & a_{42} & a_{43} & a_{44} & a_{45} & a_{46} \\ a_{51} & a_{52} & a_{53} & a_{54} & a_{55} & a_{56} \\ a_{61} & a_{62} & a_{63} & a_{64} & a_{65} & a_{66} \end{pmatrix},$$

with

$$a_{11} = r \left(1 - \frac{x_{Tn} + x_{Ts}}{\beta_T} \right) - r \frac{x_{Tn}}{\beta_T} - \delta_{mn} x_{M1} + r_{mn} x_{M2}, \quad a_{12} = -r \frac{x_{Tn}}{\beta_T} + k_{sn},$$

$$a_{13} = -\delta_{mn} x_{Tn}, \quad a_{14} = r_{mn} x_{Tn}, \quad a_{15} = 0, \quad a_{16} = 0,$$

$$a_{21} = -r \frac{x_{Ts}}{\beta_T}, \quad a_{22} = r \left(1 - \frac{x_{Tn} + x_{Ts}}{\beta_T} \right) - r \frac{x_{Ts}}{\beta_T} - k_{sn} - \delta_{ms} x_{M1} - \delta_{ts} x_{Th1},$$

$$a_{23} = -\delta_{ms} x_{Ts}, \quad a_{24} = 0, \quad a_{25} = -\delta_{ts} x_{Ts}, \quad a_{26} = 0,$$

$$a_{31} = 0, \quad a_{32} = a_s x_{M1} \left(1 - \frac{x_{M1} + x_{M2}}{\beta_M} \right), \quad a_{36} = 0,$$

$$a_{33} = (a_{m1} x_{Th1} + a_s x_{Ts}) \left(1 - \frac{2x_{M1} + x_{M2}}{\beta_M} \right) - \delta_{m1} - (k_{12} - k_{21}) x_{M2},$$

$$a_{34} = -x_{M1} \left(\frac{a_{m1} x_{Th1} + a_s x_{Ts}}{\beta_M} + k_{12} - k_{21} \right),$$

$$a_{35} = a_{m1} x_{M1} \left(1 - \frac{x_{M1} + x_{M2}}{\beta_M} \right),$$

$$a_{41} = a_n x_{M2} \left(1 - \frac{x_{M1} + x_{M2}}{\beta_M} \right), \quad a_{42} = 0,$$

$$a_{43} = -\frac{(a_{m2} x_{Th2} + a_n x_{Tn}) x_{M2}}{\beta_M} + (k_{12} - k_{21}) x_{M2},$$

$$a_{44} = (a_{m2} x_{Th2} + a_n x_{Tn}) \left(1 - \frac{x_{M1} - 2x_{M2}}{\beta_M} \right) - \delta_{m2} + (k_{12} - k_{21}) x_{M1},$$

$$a_{45} = 0, \quad a_{46} = a_{m2} x_{M2} \left(1 - \frac{x_{M1} + x_{M2}}{\beta_M} \right),$$

$$a_{51} = 0, \quad a_{52} = 0, \quad a_{53} = a_{h1} + r_{h1} x_{Th1} \left(1 - \frac{x_{Th1} + x_{Th2}}{\beta_{Th}} \right), \quad a_{54} = 0,$$

$$a_{55} = r_{h1} x_{M1} \left(1 - \frac{2x_{Th1} + x_{Th2}}{\beta_{Th}} \right) - \delta_{h1}, \quad a_{56} = -\frac{r_{h1} x_{M1} x_{Th1}}{\beta_{Th}},$$

$$a_{61} = 0, \quad a_{62} = 0, \quad a_{63} = 0, \quad a_{64} = a_{h2} + r_{h2} x_{Th1} \left(1 - \frac{x_{Th1} + x_{Th2}}{\beta_{Th}} \right)$$

Table A6

Percentage of change in tumour size on day 20 (columns 4 ND 6), for simulations with different parameter values. Columns 1 and 2 show, respectively, the baseline values of parameters that appear in model (1) and the range within which they are varied. Columns 3 and 5 show the parameter values that lead to the max decrease/increase in tumour population on day 20.

Baseline param. values	Simulation range	Param. for max % decrease	Max % decrease tumour size	Param. for max % increase	Max % increase tumour size
$r=0.565$	(0.113,1.6385)	0.113	-99	1.638	4
$\beta_T = 2 \times 10^9$	$(4 \times 10^8, 5.8 \times 10^9)$	4×10^8	-80	5.8×10^9	175
$k_{sn} = 0.1$	(0.02,0.29)	0.02	-21	0.29	4
$\delta_{mn} = 2 \times 10^{-6}$	$(4 \times 10^{-7}, 5.8 \times 10^{-6})$	5.8×10^{-6}	-21	4×10^{-7}	4
$\delta_{ms} = 2 \times 10^{-6}$	$(4 \times 10^{-7}, 5.8 \times 10^{-6})$	5.8×10^{-6}	-2	2.2×10^{-6}	0
$r_{mn} = 1 \times 10^{-7}$	$(2 \times 10^{-8}, 2.9 \times 10^{-7})$	2×10^{-8}	-2	2.9×10^{-7}	4
$\delta_{ts} = 5.3 \times 10^{-8}$	$(1.06 \times 10^{-8}, 1.53 \times 10^{-7})$	9.01×10^{-8}	0	1.06×10^{-8}	1
$a_s = 1 \times 10^{-6}$	$(2 \times 10^{-7}, 2.9 \times 10^{-6})$	2.90×10^{-6}	-3	2×10^{-7}	2
$a_n = 5 \times 10^{-8}$	$(1 \times 10^{-8}, 1.45 \times 10^{-8})$	1×10^{-8}	-5	1.45×10^{-7}	1
$a_{m1} = 5 \times 10^{-8}$	$(1 \times 10^{-8}, 1.45 \times 10^{-8})$	1.45×10^{-7}	0	1×10^{-8}	0
$a_{m2} = 5 \times 10^{-8}$	$(1 \times 10^{-8}, 1.45 \times 10^{-8})$	1×10^{-8}	0	1.45×10^{-7}	0
$\beta_M = 1 \times 10^5$	$(2 \times 10^4, 2.9 \times 10^5)$	5×10^4	-12	2.9×10^5	6
$\delta_{m1} = 0.2$	(0.04, 0.58)	0.04	-1	5.8×10^{-1}	1
$\delta_{m2} = 0.2$	(0.04, 0.58)	0.58	-12	4×10^{-2}	3
$k_{12} = 5 \times 10^{-5}$	$(1 \times 10^{-5}, 1.5 \times 10^{-4})$	2.5×10^{-5}	-42	1.45×10^{-5}	5
$k_{21} = 4 \times 10^{-5}$	$(8 \times 10^{-6}, 1.16 \times 10^{-5})$	6.8×10^{-5}	-42	8×10^{-6}	5
$a_{h1} = 8 \times 10^{-3}$	$(1.6 \times 10^{-3}, 2.32 \times 10^{-3})$	1.36×10^{-2}	0	1.6×10^{-3}	1
$a_{h2} = 8 \times 10^{-3}$	$(1.6 \times 10^{-3}, 2.32 \times 10^{-3})$	1.6×10^{-3}	0	2.32×10^{-2}	0
$r_{h1} = 9 \times 10^{-6}$	$(1.8 \times 10^{-7}, 2.61 \times 10^{-5})$	9.9×10^{-6}	0	1.53×10^{-5}	1
$r_{h2} = 9 \times 10^{-6}$	$(1.8 \times 10^{-7}, 2.61 \times 10^{-5})$	1.8×10^{-6}	0	2.61×10^{-5}	0
$\delta_{h1} = 0.05$	(0.01, 0.145)	0.01	0	0.145	1
$\delta_{h2} = 0.05$	(0.01, 0.145)	0.07	0	0.115	0
$\beta_{Th} = 1 \times 10^8$	$(2 \times 10^7, 2.9 \times 10^8)$	2.9×10^8	0	2×10^7	0

Table A7

Maximum decrease/increase in number of days (columns 4 and 6) to reach half the tumour size obtained on day 20 with the baseline model. Columns 1 and 2 show, respectively, the baseline values of parameters that appear in model (1) and the range within which they are varied. Columns 3 and 5 show the parameter values that lead to the max decrease/increase in the number of days to reach half the tumour population obtained on day 20 with the baseline parameter values.

Baseline param. values	Simulation range	Param. value for max decrease	Decrease in nbr. days	Param. value for max increase	Increase in nbr. days
$r=0.565$	(0.113, 1.6385)	1.63	-9	0.113	7
$\beta_T = 2 \times 10^9$	$(4 \times 10^8, 5.8 \times 10^9)$	4×10^9	-1	4×10^8	7
$k_{sn} = 0.1$	(0.02, 0.29)	0.08	0	0.02	1
$\delta_{mn} = 2 \times 10^{-6}$	$(4 \times 10^{-7}, 5.8 \times 10^{-6})$	4×10^{-7}	-1	5.8×10^{-6}	3
$\delta_{ms} = 2 \times 10^{-6}$	$(4 \times 10^{-7}, 5.8 \times 10^{-6})$	4×10^{-7}	-2	4×10^{-6}	2
$r_{mn} = 1 \times 10^{-7}$	$(2 \times 10^{-8}, 2.9 \times 10^{-7})$	2×10^{-8}	0	2×10^{-8}	0
$\delta_{ts} = 5.3 \times 10^{-8}$	$(1.06 \times 10^{-8}, 1.53 \times 10^{-7})$	1.06×10^{-8}	0	1.06×10^{-7}	1
$a_s = 1 \times 10^{-6}$	$(2 \times 10^{-7}, 2.9 \times 10^{-6})$	2×10^{-7}	0	2×10^{-7}	0
$a_n = 5 \times 10^{-8}$	$(1 \times 10^{-8}, 1.45 \times 10^{-8})$	1×10^{-8}	0	1×10^{-8}	0
$a_{m1} = 5 \times 10^{-8}$	$(1 \times 10^{-8}, 1.45 \times 10^{-8})$	1×10^{-8}	0	1×10^{-8}	0
$a_{m2} = 5 \times 10^{-8}$	$(1 \times 10^{-8}, 1.45 \times 10^{-8})$	1×10^{-8}	0	1×10^{-8}	0
$\beta_M = 1 \times 10^5$	$(2 \times 10^4, 2.9 \times 10^5)$	2×10^4	-2	8×10^4	0
$\delta_{m1} = 0.2$	(0.04, 0.58)	0.04	0	0.04	0
$\delta_{m2} = 0.2$	(0.04, 0.58)	0.04	-1	0.46	3
$k_{12} = 5 \times 10^{-5}$	$(1 \times 10^{-5}, 1.5 \times 10^{-4})$	8.5×10^{-5}	-3	1×10^{-5}	5
$k_{21} = 4 \times 10^{-5}$	$(8 \times 10^{-6}, 1.16 \times 10^{-5})$	8×10^{-6}	-3	5.6×10^{-5}	5
$a_{h1} = 8 \times 10^{-3}$	$(1.6 \times 10^{-3}, 2.32 \times 10^{-3})$	1.6×10^{-3}	0	1.6×10^{-2}	1
$a_{h2} = 8 \times 10^{-3}$	$(1.6 \times 10^{-3}, 2.32 \times 10^{-3})$	1.6×10^{-3}	0	1.6×10^{-3}	0
$r_{h1} = 9 \times 10^{-6}$	$(1.8 \times 10^{-7}, 2.61 \times 10^{-5})$	1.8×10^{-6}	0	9.9×10^{-6}	1
$r_{h2} = 9 \times 10^{-6}$	$(1.8 \times 10^{-7}, 2.61 \times 10^{-5})$	1.8×10^{-6}	0	1.8×10^{-6}	0
$\delta_{h1} = 0.05$	(0.01, 0.145)	0.01	0	0.01	0
$\delta_{h2} = 0.05$	(0.01, 0.145)	0.01	0	0.01	0
$\beta_{Th} = 1 \times 10^8$	$(2 \times 10^7, 2.9 \times 10^8)$	2×10^7	0	2×10^7	0

$$a_{65} = -\frac{r_{h2}x_{m2}x_{Th2}}{\beta_{Th}}, \quad a_{66} = r_{h2}x_{M2} \left(1 - \frac{x_{Th1} + 2x_{Th2}}{\beta_{Th}} \right) - \delta_{h2} \quad (C.1)$$

At the TF1IP steady state, in addition to the zero components already listed in Eq. (C.1), the following components of the Jacobian matrix are also zero: $a_{13} = a_{14} = a_{21} = a_{23} = a_{25} = 0$, $a_{41} = a_{43} = a_{46} = 0$, and $a_{65} = 0$. For the baseline parameter values

used throughout this paper, eigenvalues $\lambda_1 = a_{11} > 0$ and $\lambda_2 = a_{22} > 0$ (since $x_{M1}^* \approx 5805$ and $x_{Th1}^* \approx 4333217$), and thus this state is always unstable. However, it could be possible that for different parameter values (e.g., much higher values of $\delta_{mn}, \delta_{ms}, \delta_{ts}$), $\lambda_{1,2} < 0$. Then the stability could be influenced by the sign of $\lambda_3 = a_{44} = x_{M1}(k_{12} - k_{21}) - \delta_{m2}$: $\lambda_3 > 0$ if $k = k_{12}/k_{21} > 1$, and $\lambda_3 < 0$ otherwise.

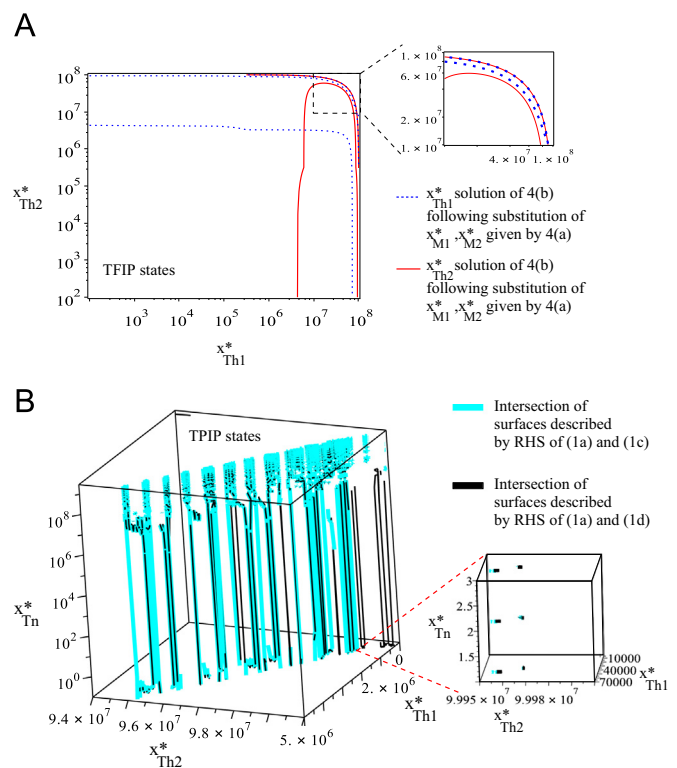


Fig. B1. Multiple TFIP and TPIP steady states. (A) The states x_{Th1}^* and x_{Th2}^* of the TFIP steady states (see Eq. (4), for $k = k_{12}/k_{21} = 1.2$). The inset shows a detailed picture of these states for $x_{Th1}^*, x_{Th2}^* \in (10^7, 10^8)$. The overlap of the continuous and dotted curves, for all x_{Th1}^* and x_{Th2}^* values within this interval, suggest the possibility of having an infinite number of steady states. (B) The TPIP states with $x_{Tn}^* = 0$ are given by the intersection of the surfaces described by the right-hand sides (RHS) of Eqs. (1a) and (1c) (cyan curves; grey in black/white print) and RHS of Eqs. (1a) and (1d) (black curves). Here, we consider $k = k_{12}/k_{21} = 5$ (although different k generate similar curves). Note that there seems to be an infinite number of intersection points between the cyan and black curves. The inset shows the intersection points for $x_{Tn}^* \in \{1, 2, 3\}$.

At the TF2IP steady state, in addition to the zero components listed in Eq. (C.1), the following components of the Jacobian matrix are also zero: $a_{13} = a_{14} = 0$, $a_{21} = a_{23} = a_{25} = 0$, $a_{32} = a_{34} = a_{35} = 0$, and $a_{56} = 0$. Since eigenvalue $\lambda_1 = x_{M2}^* r_{mn} + r > 0$, the TF2IP state is always unstable.

The stability of the multiple TFIP steady states is difficult to investigate: e.g., one of the eigenvalues of the Jacobian matrix is $\lambda_1 = a_{11} = -x_{M1} \delta_{mn} + x_{M2} r_{mn} + r$. As shown in Fig. B1(A), some states have $x_{M1} \gg x_{M2}$ and hence $\lambda_1 < 0$, while other states have $x_{M1} \ll x_{M2}$ and hence $\lambda_1 > 0$.

The TO steady state is always unstable for the parameter values used in this paper (since one eigenvalue is $\lambda_1 = x_{Tn} a_n - \delta_{m2} > 0$).

For the TP1IP state, in addition to the zero components in Eq. (C.1), the following components of the Jacobian matrix are also zero: $a_{21} = a_{23} = a_{25} = 0$, $a_{41} = a_{43} = a_{46} = 0$, and $a_{65} = 0$. The stability of this state is governed by the following eigenvalues: $\lambda_1 = a_{11} < 0$, $\lambda_2 = a_{22} < 0$, $\lambda_3 = a_{44} = 90.213 + 5805.95(k_{12} - k_{21})$, $\lambda_4 = a_{66} < 0$ and $\lambda_{5,6} = 0.5(a_{33} + a_{55}) \pm 0.5\sqrt{(a_{33} + a_{55})^2 - 4(a_{33}a_{55} - a_{35}a_{53})}$. For the baseline parameter values used throughout this paper, $k = k_{12}/k_{21} = 1.2 > 1$ which implies that $\lambda_3 > 0$ and this state is unstable.

For the TP2IP state, in addition to the zero components in Eq. (C.1), the following components of the Jacobian matrix are also zero: $a_{21} = a_{23} = a_{25} = 0$, $a_{32} = a_{34} = a_{35} = 0$, and $a_{56} = 0$. The stability of this state is governed by the sign of the following eigenvalues: $\lambda_1 = a_{22} < 0$, $\lambda_2 = a_{33} = -0.2 - 99808.35(k_{12} - k_{21})$, $\lambda_3 = a_{55} < 0$ and $\lambda_{4,5,6} < 0$ given by the three real roots of a cubic equation. If $k = k_{12}/k_{21} > 1$ then $\lambda_2 < 0$ and the TP2IP state is stable (as is the

case for the baseline model). On the other hand, if $k < 1$ then $\lambda_2 > 0$ and the TP2IP state is unstable.

The stability of the TPIP states is difficult to investigate since, as shown in Fig. B1(B), there are multiple tumour states x_{Tn}^* . However, the stability of these states also depends on the ratio $k = k_{12}/k_{21}$.

References

Baba, T., Iwasaki, S., Maruoka, T., Suzuki, A., Tomaru, U., Ikeda, H., Yoshiki, T., Kasahara, M., Ishizu, A., 2008. Rat CD4+CD8+ macrophages kill tumor cells through an NKG2D- and granzyme/perforin-dependent mechanism. *J. Immunol.* 180 (5), 2999–3006.

Bingle, L., Brown, N.J., Lewis, C.E., 2002. The role of tumour-associated macrophages in tumour progression: implications for new anticancer therapies. *J. Pathol.* 196 (3), 254–265.

Biswas, S.K., Mantovani, A., 2010. Macrophage plasticity and interaction with lymphocyte subsets: cancer as a paradigm. *Nat. Immunol.* 11 (10), 889–896.

Carmona-Fontaine, C., Bucci, V., Akkari, L., Deforet, M., Joyce, J., Xavier, J., 2013. Emergence of spatial structure in the tumor microenvironment due to the Warburg effect. *Proc. Natl. Acad. Sci. USA* 110 (48), 19402–19407.

Chen, P., Huang, Y., Bong, R., Ding, Y., Song, N., Wang, X., Song, X., Luo, Y., 2011. Tumor-associated macrophages promote angiogenesis and melanoma growth via adrenomedullin in a paracrine and autocrine manner. *Clin. Cancer Res.* 17 (23), 7230–7239.

Cillo, C., Dick, J., Ling, V., Hill, R., 1987. Generation of drug-resistant variants in metastatic B16 mouse melanoma cell lines. *Cancer Res.* 47, 2604–2608.

Clear, A.J., Lee, A.M., Calamini, M., Ramsay, A.G., Morris, K.J., Hallam, S., Kelly, G., Macdougall, F., Lister, T.A., Gribben, J.G., 2010. Increased angiogenic sprouting in poor prognosis FL is associated with elevated numbers of CD163+ macrophages within the immediate sprouting microenvironment. *Blood* 115 (June (24)), 5053–5056.

Diefenbach, A., Jensen, E.R., Jamieson, A.M., Raulet, D.H., 2001. Rae1 and H60 ligands of the NKG2D receptor stimulate tumour immunity. *Nature* 413 (6852), 165–171.

Dunn, G., Old, L., R.D., S., 2004. The three Es of cancer immunoeediting. *Annu. Rev. Immunol.* 22, 329–360.

Eftimie, R., Bramson, J., Earn, D., 2010. Modeling anti-tumor Th1 and Th2 immunity in the rejection of melanoma. *J. Theor. Biol.* 265 (3), 467–480.

Eikenberry, S., Thalhauser, C., Kuang, Y., 2009. Tumor-immune interaction, surgical treatment, and cancer recurrence in a mathematical model of melanoma. *PLoS Comput. Biol.* 5 (4), e1000362.

Ginhoux, F., Jung, S., 2014. Monocytes and macrophages: developmental pathways and tissue homeostasis. *Nat. Rev. Immunol.* 14 (6), 392–404.

Gordon, S., Martinez, F., 2010. Alternative activation of macrophages: mechanism and functions. *Immunology* 32, 593–604.

Gross, F., Metzner, G., Behn, U., 2011. Mathematical modelling of allergy and specific immunotherapy: Th1–Th2–Treg interactions. *J. Theor. Biol.* 269 (1), 70–78.

Hammes, L.S., Tekmal, R.R., Naud, P., Edelweiss, M.L., Kirma, N., Valente, P.T., Syranjan, K.J., Cunha-Filho, J.S., 2007. Macrophages, inflammation and risk of cervical intraepithelial neoplasia (CIN) progression—clinicopathological correlation. *Gynecol. Oncol.* 105 (1), 157–165.

Herwig, M.C., Bergstrom, C., Wells, J.R., Holler, T., Grossniklaus, H.E., 2013. M2/M1 ratio of tumor associated macrophages and ppar-gamma expression in uveal melanomas with class 1 and class 2 molecular profiles. *Exp. Eye Res.* 107, 52–58.

Heusinkveld, M., van der Burg, S.H., 2011. Identification and manipulation of tumor associated macrophages in human cancers. *J. Transl. Med.* 9, 216.

Hill, R., Chambers, A., Ling, V., Harris, J., 1984. Dynamic heterogeneity: rapid generation of metastatic variants in mouse B16 melanoma cells. *Science* 224 (4652), 998–1001.

Hung, K., Hayashi, R., Lafond-Walker, A., Lowenstein, C., Pardoll, D., Levitsky, H., 1998. The central role of CD4(+) T cells in the antitumor immune response. *J. Exp. Med.* 188 (12), 2357–2368.

Kim, Y., Lee, S., Kim, Y., Lawler, S., Gho, Y., Kim, Y., Hwang, H., 2013. Regulation of Th1/Th2 cells in asthma development: a mathematical model. *Math. Biosci. Eng.* 10 (4), 1095–1133.

Kisseleva, E., Becker, M., Lemm, M., Fichtner, I., 2001. Early macrophage and cytokine response during the growth of immunogenic and non-immunogenic murine tumours. *Anticancer Res.* 21 (5), 3477–3484.

Kogan, Y., Agur, Z., Elishmereni, M., 2013. A mathematical model for the immunotherapeutic control of the Th1/Th2 imbalance in melanoma. *Discrete Contin. Dyn. Syst.* 18 (4), 1017–1030.

Kuroda, M., 2010. Macrophages: do they impact AIDS progression more than CD4 T cells? *J. Leukoc. Biol.* 87, 569–573.

Laird, A., 1964. Dynamics of tumor growth. *Br. J. Cancer* 18, 490–502.

Leek, R.D., Lewis, C.E., Whitehouse, R., Greenall, M., Clarke, J., Harris, A.L., 1996. Association of macrophage infiltration with angiogenesis and prognosis in invasive breast carcinoma. *Cancer Res.* 56 (October (20)), 4625–4629.

Louzoun, Y., Xue, C., Lesinski, G., Friedman, A., 2014. A mathematical model for pancreatic cancer growth and treatments. *J. Theor. Biol.* 351, 74–82.

- 1 Ma, J., Liu, L., Che, G., Yu, N., Dai, F., You, Z., 2010. The M1 form of tumor-associated
2 macrophages in non-small cell lung cancer is positively associated with survival
3 time. *BMC Cancer* 10, 112–120.
- 4 Mantovani, A., Romero, P., Palucka, M., 2008. Tumour immunity: effector response
5 to tumour and role of the microenvironment. *Lancet* 371, 771–783.
- 6 Mantovani, A., Sica, A., Sozzani, S., Allavena, P., Vecchi, A., Locati, M., 2004. The
7 chemokine system in diverse forms of macrophage activation and polarisation.
8 *Trends Immunol.* 25 (12), 771–783.
- 9 Mareel, M., Baetselier, P.D., Roy, F.V., 1991. *Mechanisms of Invasion and Metastasis*.
10 CRC Press.
- 11 Mattes, J., Hulett, M., Xie, W., Hogan, S., Rothenberg, M., Foster, P., Parish, C., 2003.
12 Immunotherapy of cytotoxic T cell-resistant tumours by T helper 2 cells: an
13 eotaxin and STAT6-dependent process. *J. Exp. Med.* 197 (3), 387–393.
- 14 McCarthy, E., 2006. The toxins of William B. Coley and the treatment of bone and
15 soft-tissue sarcomas. *Iowa Orthop J.* 26, 154–158.
- 16 Mills, C.D., 2012. M1 and M2 macrophages: oracles of health and disease. *Crit. Rev.*
17 *Immunol.* 32 (6), 463–488.
- 18 Nishimura, T., Iwakabe, K., Sekimoto, M., Ohmi, Y., Yahata, T., Nakui, M., T., S., Habu,
19 S., H., T., Sato, M., Ohta, A., 1999. Distinct role of antigen-specific T helper type 1
20 (Th1) and Th2 cells in tumor eradication in vivo. *J. Exp. Med.* 190 (5), 617.
- 21 Noy, R., Pollard, J.W., 2014. Tumor-associated macrophages: from mechanisms to
22 therapy. *Immunity* 41 (1), 49–61.
- 23 Ohri, C.M., Shikotra, A., Green, R.H., Waller, D.A., Bradding, P., 2009. Macrophages
24 within NSCLC tumour islets are predominantly of a cytotoxic M1 phenotype
25 associated with extended survival. *Eur. Respir. J.* 33 (1), 118–126.
- 26 Pepper, M., Jenkins, M.K., 2011. Origins of CD4(+) effector and central memory T
27 cells. *Nat. Immunol.* 12 (6), 467–471.
- 28 Perez-Diez, A., Joncker, N., Choi, K., Chan, W., Anderson, C., Lantz, O., Matzinger, P.,
29 2007. CD4 cells can be more efficient at tumor rejection than CD8 cells. *Blood*
30 109, 5346–5354.
- 31 Ribeiro, R.M., Mohri, H., Ho, D.D., Perelson, A.S., 2002. In vivo dynamics of T cell
32 activation, proliferation, and death in HIV-1 infection: why are CD4+ but not
33 CD8+ T cells depleted? *Proc. Natl. Acad. Sci. USA* 99 (24), 15572–15577.
- 34 Romagnani, S., 1999. Th1/Th2 cells. *Inflamm. Bowel Dis.* 5 (4), 285–294.
- 35 Rosenberg, S., Yang, J., Restifo, N., 2004. Cancer immunotherapy: moving beyond
36 current vaccines. *Nat. Med.* 10 (9), 909–915.
- 37 Schreiber, R.D., Old, L.J., Smyth, M.J., 2011. Cancer immunoediting: integrating
38 immunity's roles in cancer suppression and promotion. *Science* 331 (6024),
39 1565–1570.
- 40 Sica, A., Bronte, V., 2007. Altered macrophage differentiation and immune dys-
41 function in tumor development. *J. Clin. Investig.* 117 (5), 1155–1166.
- 42 Sica, A., Mantovani, A., 2012. Macrophage plasticity and polarization: in vivo veritas.
43 *J. Clin. Investig.* 122 (3), 787–795.
- 44 Steidl, C., Lee, T., Shah, S.P., Farinha, P., Han, G., Nayar, T., Delaney, A., Jones, S.J.,
45 Iqbal, J., Weisenburger, D.D., Bast, M.A., Rosenwald, A., Muller-Hermelink, H.-K.,
46 Rimsza, L.M., Campo, E., Delabie, J., Braziel, R.M., Cook, J.R., Tubbs, R.R., Jaffe, E.S.,
47 Lenz, G., Connors, J.M., Staudt, L.M., Chan, W.C., Gascoyne, R.D., 2010. Tumor-
48 associated macrophages and survival in classic Hodgkin's lymphoma. *New Engl.*
49 *J. Med.* 362 (March (10)), 875–885.
- 50 Tang, X., Mo, C., Wang, Y., Wei, D., Xiao, H., 2013. Anti-tumour strategies aiming to
51 target tumour-associated macrophages. *Immunology* 138 (2), 93–104.
- 52 Van Furth, R., 1989. Origin and turnover of monocytes and macrophages. *Curr. Top.*
53 *Pathol.* 79, 125–150.
- 54 Wang, Y., Yang, T., Ma, Y., Halade, G., Zhang, J., Lindsey, M., Jin, Y.-F., 2012. Mathe-
55 matical modelling and stability analysis of macrophage activation in left ven-
56 tricular remodelling post-myocardial infarction. *BMC Genom.* 13 (Suppl. 6).
- 57 Welsh, T., Green, R., Richardson, D., Waller, D., O'Byrne, K., Bradding, P., 2005.
58 Macrophage and mast-cell invasion of tumor cell islets confers a marked sur-
59 vival advantage in non-small-cell lung cancer. *J. Clin. Oncol.* 23 (35),
60 8959–8967.
- 61 Xu, W., Liu, L., Loizidou, M., Ahmed, M., Charles, I., 2002. The role of nitric oxide in
62 cancer. *Cell Res.* 12 (5–6), 311–320.
- 63 Zeni, E., Mazzetti, L., Miotto, D., Lo, C., Maestrelli, P., Querzoli, P., Pedriali, M., De
64 Rosa, E., Fabbri, L., Mapp, C., Boschetto, P., 2007. Macrophage expression of
65 interleukin-10 is a prognostic factor in nonsmall cell lung cancer. *Eur. Respir.*
66 30, 627–632.
- 67 Zhang, M., He, Y., Sun, X., Li, Q., Wang, W., Zhao, A., Di, W., 2014. A high M1/M2 ratio
68 of tumor-associated macrophages is associated with extended survival in
69 ovarian cancer patients. *J. Ovarian Res.* 7, 19.
- 70 Zijlman, H.J.M.A.A., Fleuren, G.J., Baelde, H.J., Eilers, P.H.C., Kenter, G.G., Gorter, A.,
71 2006. The absence of CCL2 expression in cervical carcinoma is associated with
72 increased survival and loss of heterozygosity at 17q11.2. *J. Pathol.* 208 (March
73 (4)), 507–517.